



Petrography and chemistry of chromite phases from the Mesoarchean chromitite bodies of the Boula-Nuasahi ultramafic complex, India: Indicators of magmatic evolution and hydrothermal alteration

Bibhuranjan Nayak^{1,2} · Rojalini Debata^{1,2} · Kamali Kesavan^{1,2} · Ashutosh Rath^{1,2} · Lars H. Gronen^{3,4} · Sven Sindern³ · Thomas Wagner³

Received: 12 August 2023 / Accepted: 3 April 2024 / Published online: 17 May 2024
© The Author(s), under exclusive licence to Springer-Verlag GmbH Austria, part of Springer Nature 2024

Abstract

Occurrence of “ferrian chromites” have earlier been reported from the Mesoarchean chromite deposits in the Boula-Nuasahi ultramafic complex (BNUC) of India. We have investigated the chromitite bodies in the southern part of the BNUC (i.e., Bangur area) with respect to the mode of occurrence, petrography, chemistry and structure of the chromite types. Although morphologically five varieties of chromite ore were found, chemically only three types of chromite can be distinguished based on EPMA analysis. These are: 1) Type I: magnesiochromite [high Cr₂O₃ (57–65 wt.%), low iron (FeO: 13–17 wt.%), X^{Fe³⁺}: <0.1 apfu]; 2) Type II: ferrian chromite [moderate Cr₂O₃ (43–53 wt.%), high iron (FeO: 27–30 wt.%), X^{Fe³⁺}: 0.1 to 0.5 apfu]; and 3) Type III: ferrichromite [low Cr₂O₃ (19–29 wt.%), very high iron (FeO: 55–67 wt.%), X^{Fe³⁺}: 0.5 to 1.0 apfu]. Stoichiometrically calculated Fe₂O₃ content is very high in some grains (maximum 47 wt.%). Geochemical discrimination diagrams for the Type I pristine magnesiochromite suggest a dominantly boninitic parental magma. Trace element data obtained from LA-ICP-MS indicate that the Type II chromite has formed from a more evolved magma and is richer in trace elements such as V, Mn, Co, Cu, Pb, Ga, and Nb whereas the Type III ferrichromite shows unusually high Ti and erratic high concentrations of trace elements. Alterations in chromite is noticed in two different thermal regimes: 1) 100–200 °C related to serpentinization of dunite and peridotite rocks where chromite grains show an unaltered core, an intermediate ferrian chromite rim and an outer magnetite rim; 2) 500–600 °C where the entire chromite grain is converted to ferrichromite which can be linked to later intrusion of the Bangur gabbro. While HR-TEM study reveals that all three chromite-types have face-centered cubic structure, Raman spectroscopy indicates that there is a gradual transition of the structural state from normal spinel structure (Type I) through Type II to a fully inverse spinel structure in case of ferrichromite.

Keywords Chromite · Ultramafic complex · Magmatic evolution · Hydrothermal alteration · Mesoarchean · Boula-Nuasahi

Introduction

Chromite, Fe²⁺Cr₂O₄, is the principal ore mineral of chromium in magmatic ore deposits and it can have a wide range of compositional variation because of multiple cationic substitutions that involve e.g. Ti, Mn, Mg, Al, Fe, Zn. However, substitution of Fe³⁺ for Cr³⁺ can occur to a larger extent which gives rise to iron-rich chromite generically known as “ferrian chromite” (or ferritchromite). These compositional changes in chromite can occur during the magmatic crystallization stage or during the post-magmatic hydrothermal alteration and metamorphism. Moreover, the hydrothermal alteration could occur in different temperature regimes (low-temperature serpentinization to high-temperature magmatic events). Besides the major-element compositions, the trace-elements in chromite could throw some light on their genetic

Editorial handling: Q. Shu

✉ Bibhuranjan Nayak
brn69@rediffmail.com; bibhu@immt.res.in

- ¹ CSIR - Institute of Minerals and Materials Technology, Bhubaneswar 751013, India
- ² Academy of Scientific and Innovative Research (AcSIR), Ghaziabad 201002, India
- ³ Institute of Applied Mineralogy and Economic Geology, RWTH Aachen University, D-52056 Aachen, Germany
- ⁴ FEhS Building Materials Institute e.V. DE, Bliersheimer Strasse 62, D-47229 Duisburg, Germany

aspects. Therefore, it is pertinent to investigate the chromite-chemistry with respect to major-, minor-, and trace elements, especially in chromite deposits where both chromite and ferrian-chromite occur and chromite exhibits various morpho-types. It is also desirable to find out if there are any changes in the chromite structure due to cationic/elemental substitutions. In majority of the chromite deposits, reports on such structure-chemistry relationships are not available in public domain. In this context, the Mesoarchean chromite deposits of the Boula-Nuasahi ultramafic complex (BNUC) situated at the south-eastern flank of the Singhbhum Craton, India (Fig. 1), could serve as a perfect destination to establish such structure-chemistry relationships where ferrian chromite has been reported to occur to a considerable extent in addition to magnesian chromite. The chromitite bodies in the BNUC that are being mined since 1943 (Mukherjee

1962) have been investigated in a number of previous studies (Chakraborty 1958; Mukherjee 1962; Mohanty and Sahoo 1989; Mohanty et al. 1996, 2001; Mondal et al. 2001, 2006; Augé and Lerouge 2004; Khatun et al. 2014). The petrographic and chemical compositions of chromite and related spinel-supergrain minerals have also been studied. However, most of these studies have focused on the northern and central part of this N-S trending mafic-ultramafic belt. The Bangur chromite mining area that occurs in the S-SE of the BNUC has been studied to a lesser extent. Although the broad chemistry of chromite and related phases of this ultramafic belt is known, there is hardly any data on the trace-element content and on the structure of different types of chromite and related phases which can throw some light on their origin. The structure-chemistry relationships of chromite phases in the BNUC area are not known. High

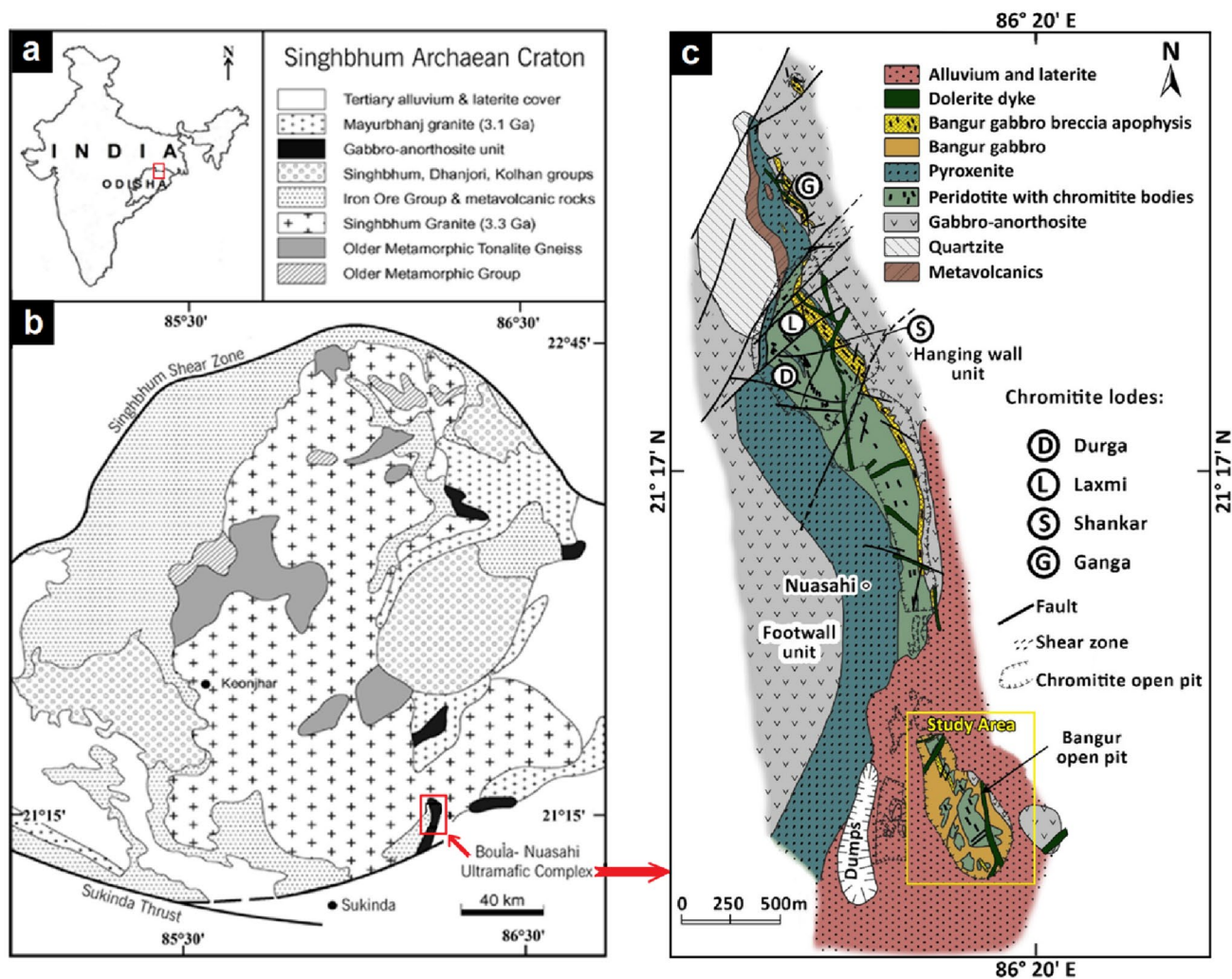


Fig. 1 Geological setting of the Boula-Nuasahi ultramafic complex (BNUC). **a** Location of the Singhbhum Archean Craton; **b** Simplified geological map of the Singhbhum Archean Craton showing

location of BNUC (modified after Saha 1994; Mondal et al. 2001); and **c** Geological map of the BNUC indicating the Bangur study area (modified after Augé et al. 2002a, b; Augé and Lerouge 2004)

Ti contents (up to 2.73 wt.% TiO₂) in chromite compositions of BNUC were reported in some variety of chromite (Mohanty et al. 2001; Augé and Lerouge 2004). However, there is neither any explanation for the high Ti-content nor the earlier workers had any discussion on its mobility and genetic implications. Hydrothermal alterations of chromite and their thermal regimes are also not very clear. There are knowledge gaps on the chemical compositional variation of chromite phases, their structure and origin. The questions that remain to be addressed are—whether the so-called ‘ferrian chromite’ is magmatic or hydrothermal? What could be the magma-type from which the chromitite bodies were formed? Therefore, we have focused on these aspects and in this paper, we present the petrographic features of chromite and related spinel-supergroup minerals, their major- and trace element chemistry, crystal structure, and alterations that are found in the Bangur area. Our study also reveals the genetic relationships between different textural types of chromite, their chemistry, and structural state.

Geological setting of the chromitite bodies

The BNUC has been emplaced into the regionally metamorphosed greenschist facies metasedimentary rocks of the Precambrian Iron-Ore Group of India (> 3.1–3.3 Ga; Mukhopadhyay 2001). The mafic-ultramafic rocks of this area form an elongate body (~3 km long and 0.5 km wide) trending NW-SE in its northern part and N-S in the southern part (Fig. 1). The major lithostructural units of this area are 1) an extensive gabbro-anorthosite suite; 2) a peridotite unit that hosts chromitite layers; 3) a pyroxenite unit; and 4) a very coarse-grained gabbro unit known as the Bangur gabbro. Although the massive and homogenous pyroxenite unit shows field relationships of partially cross-cutting the peridotite at the western edge of the peridotite unit, the first three units appear to have been emplaced coherently as part of the same magmatic cycle. By contrast, the Bangur gabbro has a clearly discordant relationship and it intrudes into the other three units in the southern part of the complex. It is a very coarse-grained pegmatoid gabbro-norite that consists of euhedral cumulus plagioclase, orthopyroxene and clinopyroxene crystals (up to 1 cm) and contains xenoliths of dunite and chromitite of variable size and shape incorporated from the host ultramafic unit (Fig. 2). Locally, the chromitite xenoliths within the Bangur gabbro have the shape of nodules ranging in diameter from less than 1 cm to more than 10 cm. This gabbro unit also has an extended NW-trending breccia apophysis which is narrow, curvilinear and about 2 km long. Because of the intrusion of the Bangur gabbro, the lithological sequence in the southern part (i.e., Bangur area) has been structurally disturbed. The BNUC is also transected by a network of Proterozoic dolerite and

ultramafic dykes and younger NNE-trending crosscutting faults (Saha 1994).

On the western footwall side of the complex, the medium-grained gabbro-anorthosite unit includes pyroxene-rich gabbro, olivine gabbro, norite, anorthosite, and layers of titanium-ferrous and vanadiferous magnetite (Chatterjee 1945). The gabbro on the eastern hanging wall side is predominantly massive and fine-grained. The intrusive Bangur gabbro was injected into a shear zone, giving rise to a magmatic breccia that cuts the ultramafic unit obliquely; it also cuts the gabbro-anorthosite unit. The breccia clasts are mainly blocks composed of host dunite, pyroxenite or chromitite, depending on the unit affected by shearing. The chromitite layers were progressively fragmented into smaller pieces and gradually incorporated into the gabbro matrix during the brecciation process. A detailed description of the breccia zone has been given by Mondal et al. (2001). The formation of the breccia was followed by late magmatic hydrothermal activity within the gabbro matrix causing alteration of Fe-Mg silicates into hydrous phases such as amphibole and mica, and partial alteration of the chromite to ferrian chromite (Augé et al. 2002b; Augé and Lerouge 2004). The hydrothermal activity is manifested by base-metal sulphide mineralization which is associated with significant PGE concentrations as well.

In the northern and central part of BNUC, four chromitite units have been recognized that are locally named as Durga, Laxmi, Shankar and Ganga (Fig. 1). The chromitite units occur as layers, lenses and veins of varying shape and dimension. Confined to the dunite and peridotite rocks, the chromite ore bodies occur as steeply inclined layers or veins. The description of different chromitite units can be found in Augé et al. (2002b). However, in the present study area (i.e., Bangur chromite mines) no such distinction can be made. Due to structural disturbance the entire Bangur area is fractured, faulted and brecciated and consists of dislodged and fragmented chromitite bodies. The typical magmatic breccia is also locally observable.

Samples and methods

Sample collection and specimen preparation

Samples of chromitite and associated rock types were collected from Bangur chromite mines; both from the old non-operational open pit and the working underground mines at +30 mRL. Sample weights vary from ~2 to 4 kg and each sample consisted of rock fragments ~8 to 15 cm. From each sample a characteristic piece was taken and was cut to desired size in billet shape by using a cutting machine fitted with diamond saw embedded with shards of diamond. Further thinning of the rock slice was done using a slow-speed cutting machine. Polished thin sections of

Fig. 2 **a** Gabbro-anorthosite rock near the opencast Bangur mining area; **b** Alternate layers/bands of dunite and chromitite that are faulted (underground mines at +30 mRL), the scale is 30 cm; **c** Field photograph showing the brecciated zone on the surface; **d** Sub-rounded chromitite clasts embedded within the brecciated ultramafic rocks; **e** A chromitite boulder within highly altered ultramafics near top bench of Bangur opencast mine; the scale is 30 cm; **f** both dunite boulders and gabbro matrix have been severely altered to serpentinite and chloritite respectively near Nuasahi in the Bangur gabbro breccia apophysis



the samples were prepared on standard glass slides (with sample area of $\sim 20 \times 30$ mm) by conventional techniques by mounting on glass-slides in araldite, followed by grinding in abrasive emery papers (SiC) starting at 180 grit up to 1000 grit and then polishing with diamond paste (1μ and 0.3μ). Two slides were prepared from each sample.

The samples were petrographically examined using a Leica DM 4000P transmitted- and reflected-light microscope, in order to identify the ore and gangue minerals. On the same polished sections, scanning electron microscopy (SEM) studies were undertaken at CSIR-IMMT Bhubaneswar, and electron probe micro-analysis (EPMA) and Laser Ablation Inductively Coupled Plasma Mass Spectrometry (LA-ICP-MS) analyses were carried out at the Institute of Applied Mineralogy and Economic Geology (RWTH Aachen University, Germany).

Scanning electron microscopy

For SEM study, polished sections of the samples were first coated with ultra-thin film of gold by an ion sputter (Quorum SC7620 Sputter Coater) and studied using an SEM (ZEISS EVO 18) having an attachment of Energy Dispersive Spectrometer [EDAX Octane Elect EDS system having silicon drift detection (SDD) technology]. The EDS was used to determine the semi-quantitative elemental composition of the mineral phases that shows only relative abundance of the elements present in a particular mineral phase. Detectors for secondary electrons (SE) and back scattered electrons (BSE) were used to capture images. For point analysis, the SEM was operated at an accelerated voltage of 20 kV and the electron beam spot size was $\sim 1 \mu\text{m}$ diameter.

Electron-probe microanalysis

The quantitative microchemical compositions of chromite grains were determined with a JEOL JXA-8900R EPMA instrument, using wavelength-dispersive X-ray spectroscopy (WDS) equipped with six spectrometers and four different crystals (LiF, PET, ADP, TAP). The acceleration voltage was set to 20 kV, the beam current to 27 nA and the beam diameter to 1–2 μm . Measurement counting times were set to 10 s for the element peaks and 5 s for both upper and lower background. Quantitative analyses were undertaken with the help of a pre-set automatic programmable point scanner using appropriate standards and on-line ZAF correction program (standard Oxide ZAF). Electron microprobe point analysis was carried out extensively on different type of chromite phases in 13 chromitite samples (at least 20 point analyses in each sample). Fourteen elements (Si, S, V, Cr, Fe, Al, Ti, Mn, As, Ca, Ni, Mg, Cu and Zn) were included in the EPMA program and determined by the WDS. Although S, As, and Cu are generally not expected in chromite, these elements were included in the program expecting that there could be some later contamination due to late-stage magmatic-hydrothermal input by Bangur gabbro intrusion. All these elements were measured on $K\alpha$ except As ($L\alpha$). Analytical standards used in the EPMA were chromite (for Cr, Fe, Al, Mg), rutile (for Ti), Vanadium (for V), Mn-oxide (for Mn), sphalerite (for S), Nickeline (for Ni, As), cuprite (for Cu), willemite (for Zn), and labradorite (for Si). Relative analytical error is ~ 2 percent for major elements and < 10 percent for minor elements. The precision for major elements (Cr, Fe, Al and Mg) was better than 1%. Since S, As and Cu were not detected at all, these elements have not been included in the analytical report (Table 1).

LA-ICP-MS analysis

Trace element concentrations of chromite were determined on polished thin sections using LA-ICP-MS. The LA-ICP-MS system comprised a NewWave UP193FX ArF excimer laser having a standard Ablation cell and a PerkinElmer Elan DRCE quadrupole mass spectrometer. The laser parameters included: background time of 60 s, analysis duration of 50 ± 5 s, washout time 50 s, laser repetition rate 6–8 Hz, laser spot size 150 μm , irradiation rate of 0.70 GW/cm^2 and the carrier gas was He with a flow-rate of 0.6 L/min. In the Mass-spectrometer, reaction cell mode was kept off while auto lens mode was on. Other conditions maintained include – plasma RF power 1350 W, nebulizer gas 0.8 L/min Ar, plasma gas 15 L/min Ar, plasma auxiliary gas 1.2 L/min Ar. The oxide formations determined as ThO/Th which was $< 0.4\%$. Analytical and data standardization procedures were carried out using NIST 610 glass as an

external reference material for all measured elements. Precision and accuracy were monitored by regular measurement of reference materials. Iron (FeO) concentration obtained by EPMA was used as an internal standard element for quantification for normal chromite where the FeO content was low. However, for Fe-rich chromite, titanium concentration (TiO_2) obtained by EPMA was used as the internal standard. Each batch of six sample analyses were bracketed with four analyses of the NIST 610 standard. Element concentrations were calculated using the SILLS data reduction software (Guillong et al. 2008). The final analytical program included the following masses: ^{45}Sc , ^{47}Ti , ^{51}V , ^{55}Mn , ^{57}Fe , ^{59}Co , ^{60}Ni , ^{63}Cu , ^{66}Zn , ^{69}Ga , ^{72}Ge , ^{75}As , ^{90}Zr , ^{93}Nb , and ^{208}Pb .

Transmission electron microscopy

For crystallographic structural analysis, pure chromite grains were manually separated (visually under a stereomicroscope) from crushed samples of different type of ores. Chromite grains of each type were ground to a fine powder with agate mortar and pestle, dispersed in ethanol, and transferred to carbon-coated Cu-grids. Crystallographic investigation was performed at CSIR-Institute of Minerals and Materials Technology (CSIR-IMMT), Bhubaneswar with a JEOL-JEM 200 F High-resolution Transmission Electron Microscope (HRTEM) operated at 200 kV. Bright-field (BF) low-magnification TEM imaging (using a 40-micron objective lens aperture), selected area electron diffraction (SAED) (using the 40-cm camera length and 50-micron aperture) and corresponding fast Fourier transform (FFT) were obtained to investigate the structure of different chromite phases.

Raman spectroscopy

Raman spectroscopic measurements were carried out on different types of chromite grains at CSIR-IMMT using a Renishaw inVia micro-Raman spectrometer equipped with an automated scanning stage. Samples were studied with 532 nm laser line emission of a frequency-doubled Nd:YAG laser. The spectrometer has a spectral resolution of 2 cm^{-1} . A $50\times$ objective (0.55 NA) was used for all the measurements. Raman spectra were recorded with the excitation laser beam in focus at the surface of the sample. A $50\times$ objective provides a focused laser beam of $\sim 2 \mu\text{m}$ in diameter. A reduced laser power of $\sim 5 \text{ mW}$ was used for experiments because high excitation laser power may cause local heating which can alter the structural state of the sample. Raman spectra were recorded at the rim and centre of different grains of chromite to observe the homogeneity and were repeated for reproducibility. The typical acquisition time for each Raman spectrum was about 60 s for each spot. The Raman spectra and compositional data were obtained from the same grain of each sample.

Table 1 Selected chromite phase compositions as measured in EPMA and their structural cationic distribution (apfu)

		Magnesiochromite (Type I)										
Sample		Massive		Spotted		Banded		Disseminated				
		R-4		R-22		R-21		R-20				
Probe No	LLD (wt.%)	15	8	2	3	9	10	11	12			
SiO ₂	0.0099	0.01	0.01	0.05	0.02	0.91	0.08	0.01	0.01			
V ₂ O ₃	0.0089	0.08	0.08	0.08	0.07	0.09	0.09	0.08	0.11			
Cr ₂ O ₃	0.0166	65.45	61.05	59.85	60.00	56.89	57.72	58.98	59.22			
FeO ^(T)	0.0115	13.49	13.69	15.67	15.77	15.82	15.86	16.73	16.82			
Al ₂ O ₃	0.0100	7.37	10.39	10.27	10.14	11.75	11.88	10.25	10.57			
TiO ₂	0.0094	0.15	0.17	0.17	0.16	0.17	0.19	0.16	0.17			
MnO	0.0101	0.54	0.24	0.30	0.26	0.26	0.28	0.30	0.31			
CaO	0.0091	0.01	0.00	0.05	0.01	0.32	0.05	0.00	0.01			
NiO	0.0094	0.07	0.11	0.06	0.08	0.07	0.08	0.05	0.04			
MgO	0.0128	13.11	14.38	12.82	12.60	13.08	13.17	12.55	12.52			
ZnO	0.0141	0.08	0.03	0.05	0.03	0.05	0.06	0.01	0.03			
Total		100.43	100.41	99.61	99.38	99.72	99.75	99.43	100.09			
No of Cations (on the basis of 3 cations)												
Si		0.0004	0.0004	0.0016	0.0006	0.0293	0.0026	0.0004	0.0003			
V		0.0021	0.0020	0.0020	0.0019	0.0024	0.0022	0.0021	0.0029			
Cr		1.6871	1.5417	1.5383	1.5488	1.4456	1.4684	1.5221	1.5177			
Fe ²⁺		0.3443	0.3052	0.3658	0.3764	0.3522	0.3555	0.3796	0.3848			
Fe ³⁺		0.0234	0.0604	0.0602	0.0544	0.0731	0.0714	0.0770	0.0711			
Al		0.2833	0.3914	0.3937	0.3904	0.4454	0.4507	0.3943	0.4038			
Ti		0.0037	0.0041	0.0042	0.0040	0.0042	0.0046	0.0040	0.0042			
Mn		0.0148	0.0065	0.0083	0.0072	0.0071	0.0077	0.0082	0.0084			
Ca		0.0002	0.0000	0.0016	0.0005	0.0111	0.0018	0.0000	0.0002			
Ni		0.0017	0.0028	0.0016	0.0021	0.0018	0.0019	0.0012	0.0010			
Mg		0.6371	0.6848	0.6214	0.6131	0.6266	0.6316	0.6106	0.6049			
Zn		0.0018	0.0006	0.0012	0.0008	0.0012	0.0014	0.0003	0.0007			
Total		3.0000	3.0000	3.0000	3.0000	3.0000	3.0000	3.0000	3.0000			
Cr#		0.856	0.854	0.796	0.799	0.765	0.640	0.794	0.790			
Mg#		0.649	0.750	0.629	0.620	0.765	0.640	0.617	0.611			
		Ferrian chromite (Type II)				Ferrichromite (Type III)						
Sample		Massive				Brecciated Ore						
		R-3				R-11		BNC-1	BNC-2B		BNC-3	
Probe No		15	16	17	18	1	2	3	1	2	1	2
SiO ₂		0.01	0.01	0.01	0.01	0.00	0.01	0.01	0.01	0.19	0.02	0.01
V ₂ O ₃		0.13	0.26	0.27	0.27	0.38	0.30	0.47	0.32	0.41	0.38	0.34
Cr ₂ O ₃		52.85	45.99	45.56	45.41	23.46	19.01	16.56	30.63	32.10	30.26	32.20
FeO ^(T)		26.61	28.21	28.20	28.35	61.22	55.11	62.36	52.48	52.92	55.60	49.44
Al ₂ O ₃		9.79	13.59	13.60	13.79	5.16	3.55	3.47	8.95	9.15	8.15	8.86
TiO ₂		0.77	1.22	1.20	1.19	4.49	17.17	12.40	3.58	2.06	0.77	6.11
MnO		0.33	0.31	0.31	0.30	0.46	0.66	0.83	0.89	0.80	0.43	0.51
CaO		0.00	0.00	0.01	0.01	0.00	0.01	0.00	0.01	0.01	0.13	0.01
NiO		0.11	0.19	0.14	0.17	0.00	0.00	0.00	0.00	0.00	0.00	0.00
MgO		9.18	10.03	10.07	9.96	0.56	0.92	0.00	0.48	0.67	0.45	0.51
ZnO		0.09	0.01	0.06	0.05	0.12	0.06	0.15	0.11	0.16	0.15	0.18
Total		100.69	100.89	100.53	100.60	99.24	99.64	99.77	99.81	100.86	99.06	100.15
No of Cations (on the basis of 3 cations)												

Table 1 (continued)

Sample	Ferrian chromite (Type II)				Ferrichromite (Type III)							
	Massive				Brecciated Ore							
	R-3				R-11		BNC-1	BNC-2B		BNC-3		
Probe No	15	16	17	18	1	2	3	1	2	1	2	
Si	0.0002	0.0002	0.0004	0.0003	0.0000	0.0004	0.0005	0.0002	0.0066	0.0007	0.0002	
V	0.0034	0.0067	0.0069	0.0071	0.0113	0.0089	0.0142	0.0092	0.0117	0.0111	0.0098	
Cr	1.3867	1.1795	1.1719	1.1672	0.6884	0.5602	0.4918	0.8733	0.9032	0.8728	0.9151	
Fe ²⁺	0.5314	0.5014	0.4977	0.5033	0.9516	0.9257	0.9694	0.9435	0.9356	0.9531	0.9521	
Fe ³⁺	0.2073	0.2642	0.2698	0.2676	0.9490	0.7927	0.9895	0.6396	0.6395	0.7435	0.5341	
Al	0.3830	0.5198	0.5216	0.5287	0.2259	0.1562	0.1537	0.3806	0.3839	0.3506	0.3755	
Ti	0.0193	0.0296	0.0295	0.0291	0.1253	0.4815	0.3503	0.0970	0.0551	0.0212	0.1652	
Mn	0.0093	0.0085	0.0084	0.0082	0.0144	0.0208	0.0265	0.0271	0.0240	0.0133	0.0156	
Ca	0.0000	0.0000	0.0004	0.0004	0.0001	0.0004	0.0000	0.0005	0.0004	0.0052	0.0004	
Ni	0.0030	0.0049	0.0037	0.0044	0.0000	0.0000	0.0000	0.0000	0.0000	0.0001	0.0000	
Mg	0.4542	0.4849	0.4882	0.4824	0.0308	0.0513	0.0000	0.0260	0.0357	0.0243	0.0271	
Zn	0.0022	0.0003	0.0015	0.0013	0.0032	0.0018	0.0041	0.0028	0.0043	0.0040	0.0048	
Total	3.0000	3.0000	3.0000	3.0000	3.0000	3.0000	3.0000	3.0000	3.0000	3.0000	3.0000	
Cr#	0.784	0.694	0.692	0.688	0.753	0.782	0.762	0.696	0.702	0.713	0.709	
Mg#	0.461	0.492	0.495	0.489	0.031	0.053	0.000	0.027	0.037	0.025	0.028	

FeO^(T) Measured total Fe expressed as FeO, LLD Lower limit of detection

Results

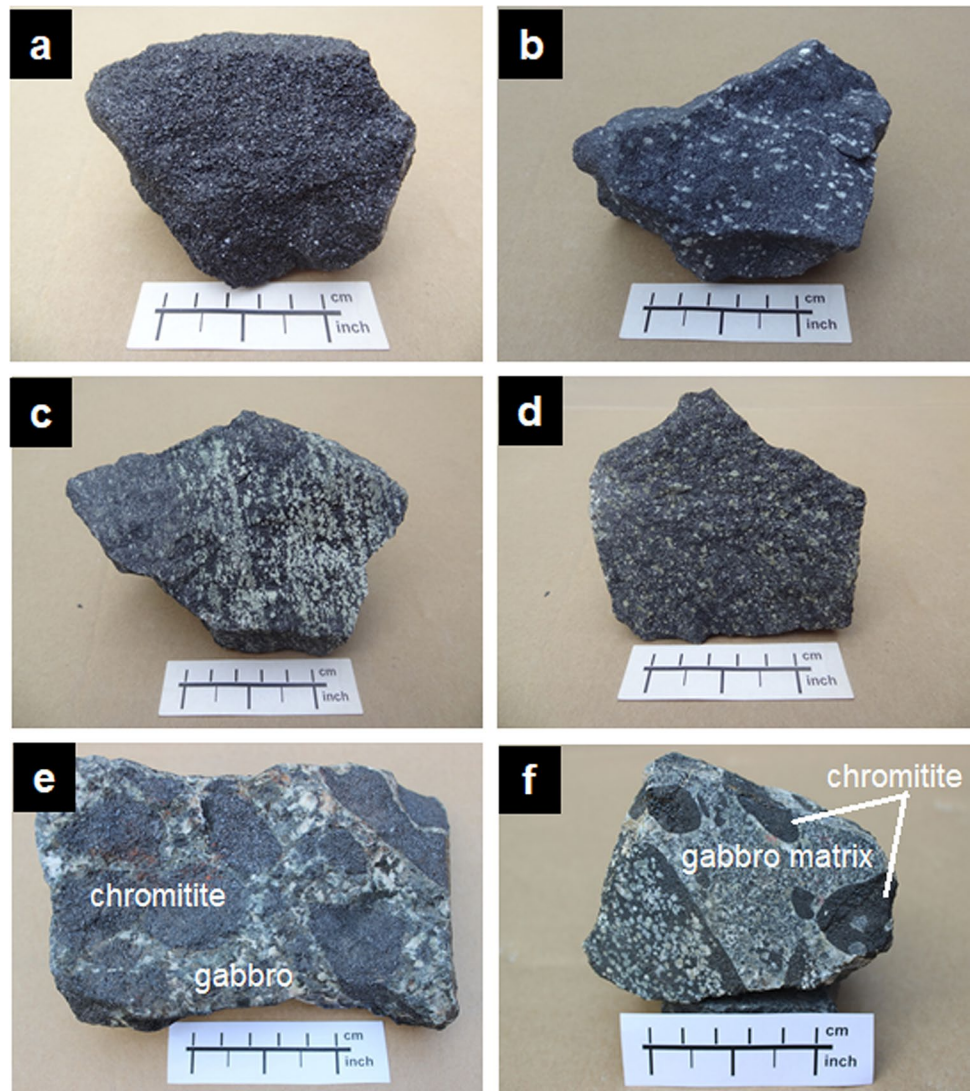
Petrography and textures of chromite

On the basis of physical appearance, five different varieties of chromite ore are identified in the Bangur area, which are the 1) massive, 2) spotted, 3) banded, 4) disseminated, and 5) breccia types (Fig. 3). The *massive* chromitite is compact, consists of closely spaced and tightly packed granular aggregates of chromite grains with very little intergranular serpentine. The chromite grains are euhedral to subhedral and vary in size from 100 to >500 µm. These chromitites show primary cumulus textures (Fig. 3a). The massive ore grades into spotted and banded types characterized by an increase in the proportion of gangue minerals. The *spotted* ore contains oval or spheroidal clots of altered silicates irregularly distributed within closely packed chromite grains giving rise to a spotted appearance to the ore (Fig. 3b). This type of ore also contains subhedral to euhedral chromite grains which vary considerably in size ranging between 30 and 600 µm. The *banded* ore contains alternating layers (sometimes quite irregular) of chromite grains and ferromagnesian silicates (Fig. 3c). The layers are of variable thickness ranging from millimeters to several centimeters. This ore contains euhedral to subhedral chromite grains which vary in size from 50 to 400 µm. The silicates are partially altered to serpentine minerals. The banded ore grades into the *disseminated*

type with a substantial increase in the proportion of gangue minerals where layering is not visible and the silicates are more abundant than chromite (Fig. 3d). The *breccia ore* is a mixed type that may contain fragments of any of the above four types or a combination of few ore types (Fig. 3e, f). It has formed as a secondary ore during the emplacement of the Bangur gabbro intrusion.

In reflected light, the chromite ores of the Bangur area show both primary magmatic textures and secondary altered structures. Massive chromitites are characterized by a foam texture where mostly coarse and euhedral chromite cumulate grains are present with straight grain boundaries, approximately equal grain size distribution and triple point junctions (Fig. 4a, b). The spotted chromitites show a chain or network texture where the small euhedral to subhedral chromite cumulate grains are joined together surrounding the areas of large cumulus silicate grains (Fig. 4c). Occasionally, along with the silicates, some fine subhedral to anhedral chromite grains are observed to fill the intergranular spaces of the large cumulus chromite grains forming a clot texture (Fig. 4d). These chromitites also exhibit cumulus texture where the subhedral to euhedral chromite cumulate grains may be connected by intercumulus silicates which are now altered (Fig. 4e). In banded ores, grain size graded layering is common (Fig. 4f). The above described textures are very common in magmatic chromite deposits and they record various stages of crystallization during cooling of

Fig. 3 Hand specimen samples of different types of chromite ores in the Bangur area. **a** Massive chromite ore; **b** Spotted type chromite ore; **c** Banded chromite ore; **d** Disseminated chromite ore; **e** Brecciated ore in which massive chromitite is embedded within coarse-grained/pegmatoid Bangur gabbro; **f** Brecciated ore in which both massive chromitite and spotted-type ore are embedded in gabbroic matrix



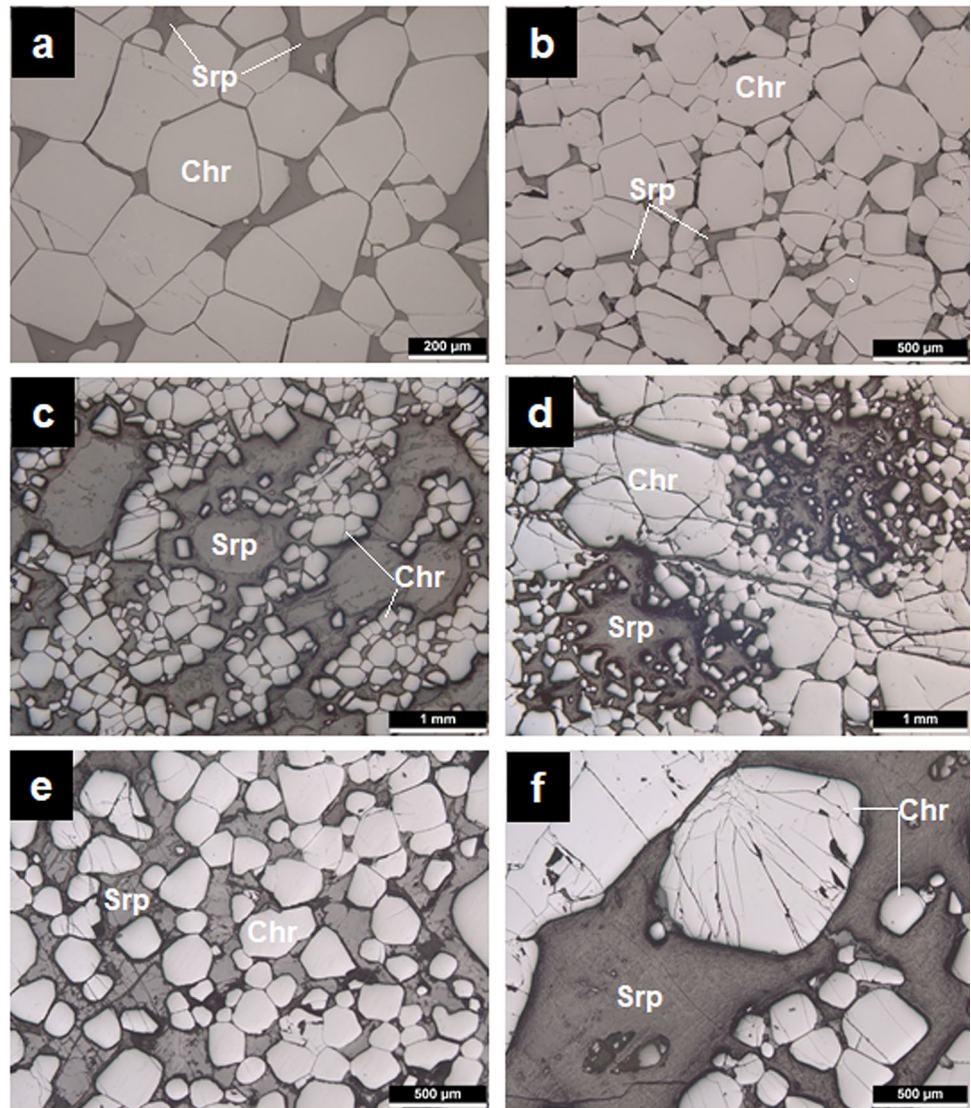
the magma, the conditions prevailing during crystallization and the magma composition (Thayer 1960; Mukherjee 1969; Stanton 1972). Apart from this, in the brecciated ores, various secondary textures such as cataclastic, replacement and other modified textures that are found in the chromite ores are illustrated in Fig. 5. This type of chromite is dominantly found in the Bangur-gabbro contact zone. Although physically these are not so clearly distinguishable from previously described chromite, they are very easily identifiable under the optical microscope. They are generally porous having a brownish grey colour and are characterized by irregular and corroded grain boundaries (Fig. 5). Sometimes these chromite phases contain inclusions of sulphides (dominantly chalcopyrite; less cubanite and pyrrhotite) that occupy fractures, pores and crystallographic planes of chromite. Rarely, the chromite grains are partially to pervasively replaced by the sulphides. In few instances, such chromite grains also contain irregular inclusions of ilmenite. In addition, there are

partially altered chromite grains which show diffuse bands with variable reflectance (Fig. 6).

Hydrothermal alteration

Alteration of original (magmatic) chromite grains has been recorded in the study area where the chromite is affected by alteration from grain boundaries and in fracture planes that gives rise to 1) an unaltered chromite core, 2) an intermediate ferrian-chromite rim, and 3) an outer magnetite rim (Fig. 6). The sharp corners of the original euhedral chromite grains are smoothed and the grains become sub-rounded to rounded. The ferrian chromite rim has a diffuse and smooth boundary with the unaltered chromite core but can have diffuse as well as sharp contacts with the outer magnetite. The outer magnetites have crystal outlines and do not have a smooth boundary with the surrounding chlorite/serpentine. This

Fig. 4 Primary textures observed in the chromitites of Bangor area under plane polarized reflected light. **a** and **b** Massive chromitites showing foam texture where mostly coarse and euhedral chromite cumulates are seen with straight grain boundaries and showing triple point junctions; **c** Spotted chromitites show synneusis (chain/network) texture where the small euhedral to subhedral chromite cumulates are joined together encircling the areas of large cumulus silicate grains; **d** Fine subhedral to anhedral chromite grains are found to fill the intergranular spaces of the large cumulus chromite grains forming clot texture; **e** Chromitites showing cumulus texture with intercumulus altered silicates; **f** Banded ores showing size graded layering. Abbreviations used for mineral names in this and all subsequent figures are as per Whitney and Evans (2010)



type of alteration is mainly observed in the altered dunite/peridotite rocks where the Fe-Mg silicates have been chloritized and/or serpentized. Such type of alteration is not recorded in massive chromitites which indicates that this type of alteration is related only to serpentization process (~100–200 °C).

In contrast to the examples described above and in the literature (e.g. Burkhard 1993) where ferrian chromite rims developed around chromite grains during low-temperature serpentization, there is another type of porous chromite (Fig. 5) which has (presumably) formed due to magmatic-hydrothermal alteration at significantly higher temperature. These chromites have a uniform brownish-grey colour (resembling magnetite) under the reflected-light microscope and are devoid of any zoning. Their grain boundaries are either semi-rounded or marginally corroded. This type of chromite is dominantly found in the brecciated ores in close proximity to the

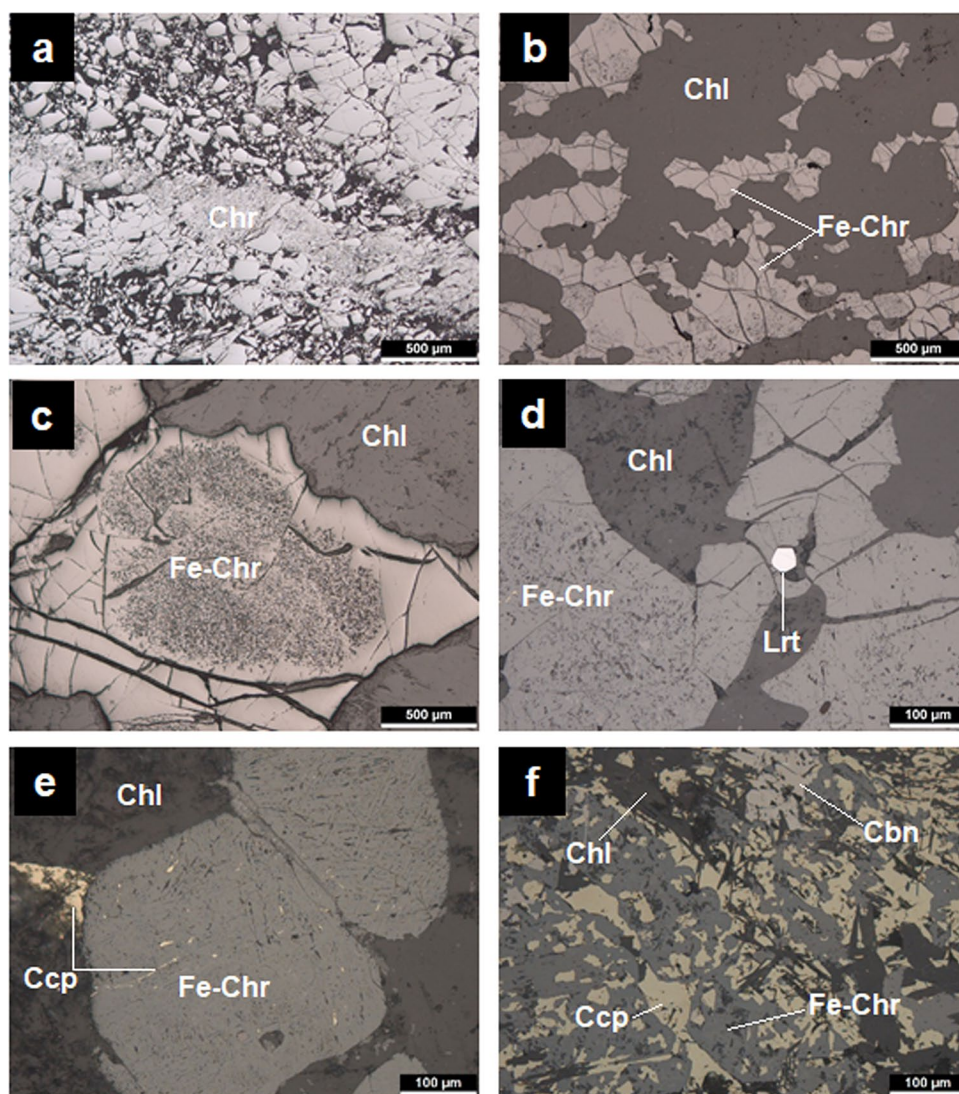
Bangor-gabbro contact zone where the earlier formed lithological units have suffered hydrothermal alteration at relatively higher temperature due to the intrusion of the Bangor Gabbro. The temperature of this high-temperature hydrothermal activity has been estimated to be at least 500–600 °C (Augé and Lerouge 2004).

Mineral chemistry of chromite phases

Major element compositions

Although macroscopically five different morphological types of chromite ore were identified (see Fig. 3), chemically only three types of chromite compositions were identified by EPMA. Selected EPMA data of chromite phases from each type are presented in Table 1. The complete dataset and a summarized data table are provided as Electronic Supplementary Material (Table 1a and Table 1b). Type

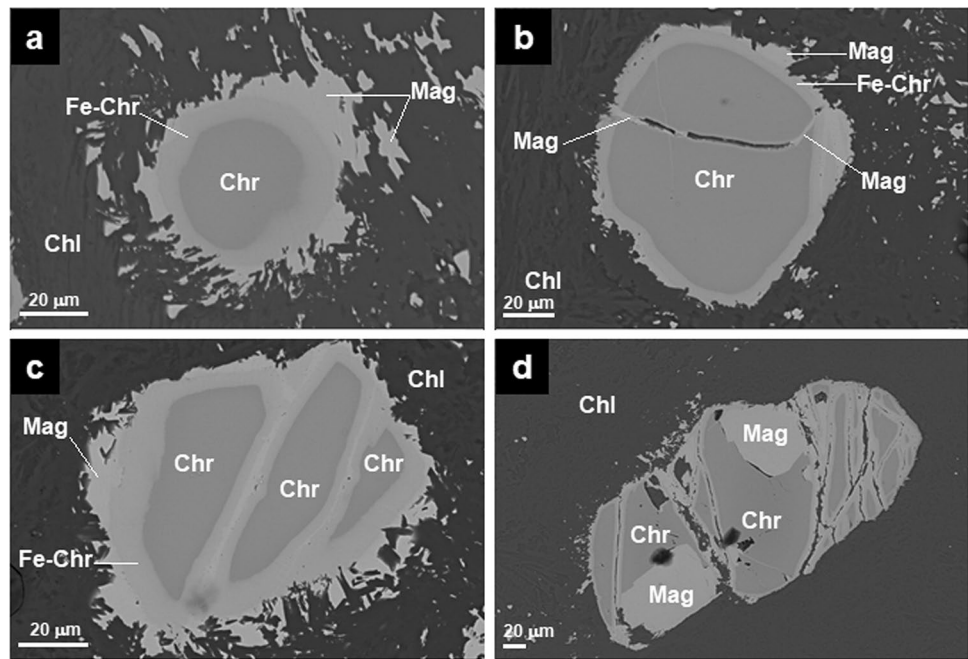
Fig. 5 Secondary textures recorded in the chromitites of Bangur area under plane polarized reflected light. **a** Cataclastic texture developed in chromitite due to brecciation where chromite grains are fractured and fragmented; **b** chromite grains are converted to ferrichromite because of hydrothermal alteration; **c** Ferrichromite showing irregular grain boundaries and pitted surface; **d** A laurite crystal (a platinum group mineral) is enclosed and associated with ferrichromite and chlorite; **e** Late-stage base-metal sulphide (chalcopyrite) associated with ferrichromite that penetrates into crystallographic planes and pores of the chromite; **f** Severely affected and partially replaced ferrichromite by late-stage sulphide mineralization. [Fe-Chr: ferrichromite, Lrt: laurite]



I compositions have high Cr_2O_3 (56.4–65.5 wt.%) with measured iron expressed as FeO (12.5–17.7 wt.%), Al_2O_3 (7.3–12.3 wt.%), MgO (11.7–14.6 wt.%); Type II contains moderate Cr_2O_3 (42.9–52.9 wt.%), FeO (26.6–29.6 wt.%), Al_2O_3 (9.8–14.7 wt.%), MgO (9.2–10.1 wt.%); and Type III contains low Cr_2O_3 (14.2–40.5 wt.%) and high iron (FeO: 43.3–73.6 wt.%) with low Al_2O_3 (1.8–10.5 wt.%) and MgO (0.0–3.0 wt.%). The structural distribution of atoms (apfu) in chromite were calculated considering three cations per formula unit (1 unit at A^{2+} site and 2 units in B^{3+} site) as per the generalised chemical formula of spinels $\text{A}^{2+}\text{B}^{3+}_2\text{O}_4$. All the divalent cations such as Mg^{2+} , Mn^{2+} , Ca^{2+} , Ni^{2+} , Zn^{2+} were assigned to the A site. The concentration of Fe^{2+} was estimated from the difference between $\sum (\text{Mg}^{2+} + \text{Mn}^{2+} + \text{Ca}^{2+} + \text{Ni}^{2+} + \text{Zn}^{2+})$ and the ideal stoichiometric value of 1 apfu in the A site. The concentration of Fe^{3+} has been estimated from the difference between the

total number Fe apfu and the Fe^{2+} apfu assigned to A site. Subsequently, the FeO and Fe_2O_3 concentrations in wt.% were calculated from the formula occupation of Fe^{2+} and Fe^{3+} , respectively. This calculated Fe_2O_3 concentration is considerably high in some grains, reaching a maximum of 47 wt.%. Type I compositions are present in massive, banded, spotted and disseminated ores and their TiO_2 content is always very low (0.11–0.24 wt.%). Only in few massive ores, the Type II compositions were recorded. They are chemically more evolved with lower Cr_2O_3 and higher TiO_2 (0.8–1.3 wt.%) and higher iron contents. While Type I and Type II chromitites represent primary magmatic compositions, the Type III composition is characteristic of the hydrothermally altered brecciated type of ore. The TiO_2 content of Type III chromite is unusually high and quite variable (0.5 to 17.17 wt.%). The V_2O_5 content systematically increases from Type I (<0.1 wt.%) to Type III (maximum of 0.7 wt.%).

Fig. 6 **a** and **b** Back-scattered SEM images showing alteration of original (magmatic) magnesiochromite grains where the chromite suffers alteration from grain boundaries that gives rise to an unaltered chromite core, an intermediate ferrian-chromite rind, and an outer magnetite rim, and also in fracture planes **c**; **d** Sometimes only magnetite is developed without an intermediate ferrian chromite rind. [Fe-Chr: ferrichromite]



While there is no significant difference in the MnO content of Type I and Type II which remains around 0.3 wt.%, MnO is slightly higher in Type III and goes up to 0.9 wt.%. In summary, the Type III chromites represent a chemically distinct compositional type characterized by low Cr₂O₃, MgO, Al₂O₃ and with very high Fe₂O₃ and TiO₂ compared to the magmatic chromites of Type I and Type II. In the literature, such high ferric iron containing chromite has been described as “*ferritchromite*” (Spangenberg 1943; Augé et al. 2002a). According to the IMA classifications all the three varieties belong to oxyspinel group [spinel subgroup (2–3); Bosi et al. 2019]. Based on the Fe³⁺ concentrations (Mindat.org), these three types of chromite can be named respectively as 1) chromite (Fe³⁺ <0.1 apfu) with the empirical formula (Fe²⁺_{0.30–0.42}Mg_{0.57–0.69})(Cr_{1.44–1.70}Fe³⁺_{0.01–0.09}Al_{0.28–0.47}Ti_{0.00–0.01})O₄, 2) ferrian chromite (Fe³⁺: 0.1–0.5 apfu) with the empirical formula (Fe²⁺_{0.50–0.53}Mg_{0.45–0.49})(Cr_{1.10–1.39}Fe³⁺_{0.21–0.30}Al_{0.38–0.56}Ti_{0.02–0.03})O₄ and 3) ferrichromite (Fe³⁺: 0.5–1.0 apfu) with the empirical formula (Fe²⁺_{0.82–0.98}Mg_{0.00–0.16})(Cr_{0.56–1.13}Fe³⁺_{0.51–1.0}Al_{0.08–0.44}Ti_{0.01–0.55})O₄. Only in few grains the calculated Fe³⁺ concentration exceeds 1.0 apfu which would then be classified as chrome-magnetite.

Chromite phases that have been affected by low-temperature hydrothermal alteration related to the serpentinization of the silicate phases show variable chemical composition within the same grain. The core commonly has the composition of magmatic chromite with high Cr, Al, and considerable Mg. In the ferrian chromite rim, there is slight reduction of Cr, substantial increase in Fe, and major reduction in Al content are observable. However, in the magnetite rim there

is practically no Mg or Al present and only a trace quantity of Cr is recorded (Please refer Electronic Supplementary Material Fig. 6S). The other observation is that magnetite is found as a secondary phase in the fractures of chromite grains and that it distinctly replaces chromite grains with shared boundaries without formation of any intermediate ferrian chromite. In contrast to this, the ferrichromites are devoid of any compositional zoning and the micro-chemical composition is almost uniform in a single grain as measured by EPMA.

Trace element composition of the chromite phases

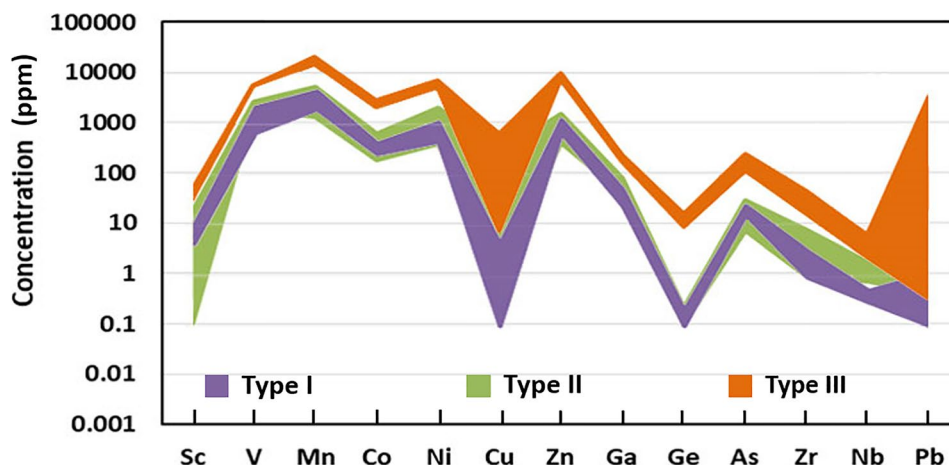
Mineral compositions of chromite from the Boula-Nuasahi area were reported by Mohanty and Sahoo 1989; Mohanty et al. 1996; Augé and Lerouge 2004 and Mondal et al. 2006. But all the earlier analytical data were limited to major and minor element compositions determined by bulk analytical techniques or by EPMA. No data on the trace element content of the chromite phases of this ultramafic belt has been previously reported. We have determined the concentrations of thirteen trace elements (Sc, V, Mn, Co, Ni, Cu, Zn, Ga, Ge, As, Zr, Nb, and Pb) by LA-ICP-MS analysis of multiple chromite grains (in total 90 different point analyses with a spot size of 150 µm) in all three textural types of chromite. A summary, comparing the trace elements data of all the three types of chromite has been presented in Table 2 and Fig. 7. Only selected analyses are presented in Table 3. All the analyses of the trace elements data are provided as Electronic Supplementary Material. The data show that the Type I chromite which represents

Table 2 Trace element concentrations ($\mu\text{g/g}$) in the three types of chromites in Bangur area (data are rounded). The detail analyses are provided in Table 3 and supplementary data sheet (Table 2b)

Chromite Type	Type I	Type II	Type III
Sc	4 - 10	<2.7 - 17	30 - 50
V	650 - 2070	1750 - 2620	5590 - 6110
Mn	1900 - 4300	1260 - 4950	14050 - 22760
Co	250 - 390	180 - 590	2020 - 3020
Ni	430 - 1000	210 - 1920	5320 - 7820
Cu	<0.9 - 4.0	<0.9 - 253	5 - 650
Zn	650 - 1170	400 - 1490	7590 - 10500
Ga	23 - 47	35 - 82	185 - 258
Ge	<6.4	<6.4	10 - 20
As	15 - 25	7 - 27	125 - 275
Zr	1 - 3	1 - 7	18 - 50
Nb	0.3 - 0.5	0.7 - 1.6	2.5 - 10.1
Pb	<0.4 - 1.1	0.4 - 95	0.4 - 3630

the original/primitive magmatic type, has generally lower concentrations of the trace elements analyzed than the Type II chromite. While the concentrations of Sc, Mn, Zn, Ge, As, Zr and Nb are somewhat comparable between Type I and Type II, the Type II clearly has higher concentrations of the other trace elements (e.g. V, Co, Cu). However, Type III chromites are exceptionally rich in all the trace elements measured and the analytical data on any specific element also vary in wide limits in different chromite grains within the same sample (e.g. V, Mn, Co, Cu, Zn, Pb). Two analyses of ferrichromite show unexpectedly high concentration of Pb (i.e., Chr 41 and Chr 49, Table 3; that's why there is a sharp rise in case of Pb in Fig. 7). This could be due to some nano-inclusions of Pb during the late-stage high-temperature hydrothermal input.

Fig. 7 Figure showing trace element concentration patterns in the three types of chromites from BNUC



Structure of the chromite phases

Transmission Electron Microscopic studies

Structural investigation through high-resolution transmission electron microscopy (HR-TEM) on isolated chromite grains reveals that all the three textural types (i.e., Types I, II and III) have the face-centered cubic (fcc) structure. Figure 8(a) shows the bright field low magnification TEM image of the pristine Type I chromite along with its corresponding selected area electron diffraction (SAED) pattern (b), and a high-resolution TEM image with corresponding fast Fourier transform (FFT) (c). The SAED reveals the d-spacings of 0.294 nm, 0.253 nm, 0.209 nm and 0.148 nm, which corresponds to the (220), (113), (400) and (440) planes of FeCr_2O_4 [JCPDS 01-089-2618]. In Fig. 8d, e, the bright field low magnification TEM image of the Type II chromite sample and related SAED shows the d-spacings of 0.484 nm, 0.294 nm, 0.253 nm, 0.209 and 0.169 nm, which corresponds to the (111), (220), (113), (400) and (224) planes of FeCr_2O_4 [JCPDS 01-089-2618]. Figure 8f shows the high-resolution TEM image and corresponding FFT (inset figure), which confirms the FeCr_2O_4 composition and the highly crystalline nature of the Type II chromite sample. In Fig. 8g, h, the bright field low magnification TEM image of the Type III chromite sample and corresponding SAED shows the d-spacings of 0.484 nm, 0.253 nm, 0.169 nm, 0.148 nm and 0.132 nm which refers to the (111), (113), (224), (440) and (602) planes of FeCr_2O_4 [JCPDS 01-089-2618]. Figure 8i shows the high-resolution TEM image and corresponding FFT which also confirms the highly crystalline nature of Type III chromite. The crystal structural data do not show any major difference in the crystal lattice structure of the texturally different chromite types.

Table 3 Trace element concentrations (µg/g) in the three types of chromites in Bangour area (data are rounded to one decimal)

Magnesiochromite (Type I)																
File	LLD	Chr 11	Chr 12	Chr 13	Chr 28	Chr 29	Chr 30	Chr 38	Chr 39	Chr 40	Chr 45	Chr 46	Chr 47	Chr 48	Chr 53	Chr 54
Sc	2.7	5.7	5.5	5.0	4.2	4.5	5.1	7.9	7.4	6.9	6.1	6.1	8.0	8.8	9.6	8.9
V	2.0	721.7	740.6	649.4	717.9	728.0	725.3	2047.1	2052.0	2067.0	1943.2	1975.2	2072.2	1788.5	1904.9	1944.8
Mn	1.7	1904.0	1934.1	2216.0	1928.6	1940.6	1940.0	4082.7	2822.5	3582.1	3884.1	2997.5	4244.9	3471.4	3452.4	3323.3
Co	1.6	307.5	314.2	247.2	311.0	315.0	316.1	335.4	284.1	300.8	271.9	259.0	386.6	371.4	363.9	354.2
Ni	5.5	695.7	699.1	430.7	645.7	657.3	682.7	844.8	784.8	746.0	705.2	685.1	890.5	881.2	960.7	1000.3
Cu	0.9	3.9	2.3	4.0	3.7	2.8	2.6	2.2	1.2	1.3	<LLD	<LLD	1.7	1.6	3.2	1.3
Zn	3.2	650.8	655.0	705.5	672.1	677.7	695.9	1048.1	895.5	989.8	791.1	792.9	1168.3	1109.5	1081.0	1059.4
Ga	1.0	23.8	23.9	25.1	24.6	24.1	23.5	37.6	35.3	35.8	33.4	31.6	39.8	40.4	45.3	47.1
Ge	6.4	<LLD	<LLD	<LLD	<LLD	<LLD	<LLD	<LLD	<LLD	<LLD	<LLD	<LLD	<LLD	<LLD	<LLD	<LLD
As	2.4	20.5	21.2	21.4	17.9	19.5	22.2	22.6	19.2	18.8	16.4	15.5	22.3	21.5	23.2	20.2
Zr	0.5	1.1	1.1	1.3	0.9	0.9	1.0	2.9	2.7	2.7	2.4	2.2	2.9	3.0	3.1	2.9
Nb	0.2	0.4	0.4	0.3	0.3	0.4	0.3	0.4	0.4	0.3	0.3	0.3	0.5	0.4	0.5	0.4
Pb	0.4	<LLD	<LLD	1.1	<LLD	<LLD	<LLD	0.4	<LLD	0.7	<LLD	<LLD	0.5	<LLD	<LLD	<LLD
Ferrian chromite (Type II)																
File	LLD	Chr 3	Chr 4	Chr 5	Chr 7	Chr 8	Chr 11	Chr 15	Chr 16	Chr 19	Chr 22	Chr 23	Chr 24	Chr 27	Chr 30	Chr 31
Sc	2.7	<LLD	2.8	3.1	<LLD	<LLD	<LLD	<LLD	<LLD	9.1	9.6	11.0	13.6	12.6	16.5	14.5
V	2.0	1968.6	2084.6	1918.4	1830.2	1876.5	2041.1	1941.9	2009.9	2247.6	2161.1	2292.2	2339.1	2616.5	2228.6	2182.6
Mn	1.7	1450.8	1530.4	1400.8	1344.0	1333.8	1472.6	1451.1	1419.3	2103.9	2891.5	4166.1	4795.4	3750.0	4951.8	4269.8
Co	1.6	196.6	223.5	191.0	181.2	203.5	212.6	200.8	202.9	286.2	358.4	452.5	545.3	453.5	584.7	505.1
Ni	5.5	519.5	418.9	507.8	499.9	376.8	378.6	463.5	489.1	1165.9	1219.1	1239.8	1893.9	1518.1	1917.2	1802.9
Cu	0.9	26.8	26.8	107.2	252.9	31.7	5.8	3.7	3.8	<LLD	<LLD	<LLD	2.1	1.0	6.9	2.4
Zn	3.2	580.5	689.0	541.3	398.8	479.3	653.3	518.7	520.4	751.0	961.9	1217.6	1487.6	1184.1	1440.4	1296.7
Ga	1.0	45.3	46.1	48.0	39.7	38.8	45.8	42.2	45.0	55.5	59.6	74.1	77.9	71.3	76.5	71.8
Ge	6.4	<LLD	<LLD	<LLD	<LLD	<LLD	<LLD	<LLD	<LLD	<LLD	<LLD	<LLD	<LLD	<LLD	<LLD	<LLD
As	2.4	12.2	12.5	12.3	17.5	8.6	8.1	7.9	7.3	16.4	20.6	24.1	27.2	23.1	25.2	21.8
Zr	0.5	4.9	3.2	2.9	1.2	0.9	5.4	4.5	3.4	6.1	4.4	3.3	6.2	5.4	7.0	7.1
Nb	0.2	1.2	1.0	1.3	1.2	0.8	1.2	1.4	1.6	0.8	0.7	0.8	0.8	1.0	0.9	0.8
Pb	0.4	10.0	94.1	24.1	3.0	7.1	8.9	27.8	40.7	1.4	3.0	3.0	0.6	2.9	0.4	0.7
Ferrichromite (Type III)																
File	LLD	Chr 37	Chr 38	Chr 39	Chr 41	Chr 42	Chr 45	Chr 49	Chr 50	Chr 53	Chr 56	Chr 57	Chr 58	Chr 61	Chr 64	Chr 65
Sc	2.7	33.8	39.9	41.2	41.2	44.1	39.1	42.0	37.8	37.2	35.4	33.2	33.9	46.3	48.3	42.1
V	2.0	5747.6	5819.0	5948.7	5588.3	5770.8	6050.9	6104.4	5763.8	6046.0	5991.5	6083.5	6107.4	5862.6	5810.6	5994.7
Mn	1.7	15477.6	18688.8	19736.8	17007.6	22389.9	20211.9	17477.1	19198.7	17098.4	18308.6	18707.2	18031.2	21422.1	21651.5	21090.7

Table 3 (continued)

Ferrichromite (Type III)																
Co	1.6	2165.2	2556.8	2687.8	2422.3	2908.8	2674.4	2439.2	2645.0	2387.7	2625.2	2577.2	2548.3	2968.8	3018.0	2894.7
Ni	5.5	6402.7	6331.6	6527.3	6804.3	7235.6	5972.0	6016.7	5577.2	6054.0	5362.3	5433.3	5328.5	7354.9	7401.5	6009.4
Cu	0.9	9.9	8.4	21.5	66.5	13.4	24.0	470.0	652.5	10.0	14.0	24.7	9.3	15.0	25.6	24.3
Zn	3.2	7733.1	8892.9	9578.1	9340.3	10505.3	9072.5	9025.0	9527.8	7845.2	8324.6	8460.8	7988.7	10202.9	9529.1	9359.0
Ga	1.0	228.7	219.4	234.6	239.9	253.7	204.7	226.1	191.3	220.3	196.5	196.2	186.8	250.6	255.6	206.0
Ge	6.4	10.3	14.6	11.7	12.9	16.1	13.3	15.4	14.6	9.7	10.7	10.9	11.1	17.6	11.4	12.1
As	2.4	247.3	243.2	231.7	220.0	229.7	267.2	237.4	249.1	228.8	155.1	127.6	151.3	135.1	153.8	166.7
Zr	0.5	19.4	23.8	24.8	28.6	33.8	21.9	19.4	19.3	17.9	21.7	20.6	22.6	39.9	49.1	27.7
Nb	0.2	4.2	5.3	4.8	6.2	5.6	4.4	4.6	4.2	3.8	2.7	2.5	2.9	6.1	6.5	4.6
Pb	0.4	1.4	44.2	256.6	3627.1	14.6	1.6	1698.7	284.2	0.9	0.4	1.1	0.6	1.7	1.1	0.9

LLD Lower limit of detection

Raman Spectroscopy

Raman spectra of Type I, Type II and Type III chromite on different grains are depicted in Fig. 9a through c, and a summary of the identified bands is given in Table 4. The strongest A_{1g} peak is generated by the internal vibration of the BO_6 octahedron where trivalent ions have a higher degree of covalence than those in $Fe^{2+}O_4$ tetrahedra. The $\nu_3(F_{2g})$ mode has also been assigned to symmetric stretching vibration of BO_6 groups. The $\nu_2(E_g)$ band corresponds to symmetric B–O stretching vibrations and the $\nu_4(F_{2g})$ band corresponds to the bending vibrations (Kharbish 2018). The lowest $F_{2g(trans)}$ lattice vibrational mode is not observed in the present study. In the Type II chromite (ferrian chromite), marginal increases in Raman shifts are observed for all bands with increasing content of the heavier Fe^{3+} ions (relative to Cr). The Raman bands of Type III chromite (ferrichromite) match well with the Raman bands of magnetite (Shebanova and Lazor 2003) indicating the inverse nature of the spinel structure in ferrichromite. Factor-group analysis for both normal and inverse spinel suggests five Raman-active vibrational modes, with the following symmetries: $A_{1g} + E_g + 3F_{2g}$ and four IR active modes $4F_{1u}$. The local distortions around the B^{3+} cations may cause a reduction in BO_6 octahedron symmetry from D_{3d} to C_{3v} and a crystal structure change from O_h to T_d , which increases the total number of Raman active modes (Table 4) (Grimes and Collett 1971).

Discussion

The composition of chromite could be modified by interaction with intercumulate melt and other coexisting minerals (e.g. Barnes 1998; Kharbish 2013). However, Mg-rich chromite (magnesiochromite) is one of the earliest minerals to crystallize from mafic melts and can be used as a petrogenetic indicator. Therefore, magnesiochromite in mafic-ultramafic rocks can provide clues to the evolution and source of its parent magmas. In the present case the three chemically distinct chromitite ores record two magmatic chromite forming stages and one late magmatic-hydrothermal stage. Chromite occurring as minor phases within dunite and peridotite rocks have also undergone low-temperature hydrothermal alteration related to serpentinization/chloritization. The major and trace element chemistry of chromite phases shows significant variations which will be interpreted in terms of primary and secondary processes, i.e. source and evolution of primary melts and hydrothermal alteration of chromite.

Source and evolution of the primary chromitite forming melts

The Type I chromite contains high Cr_2O_3 (56.4–65.5 wt.%), high MgO (11.7–14.6 wt.%), high Al_2O_3 (7.3–12.3 wt.%),

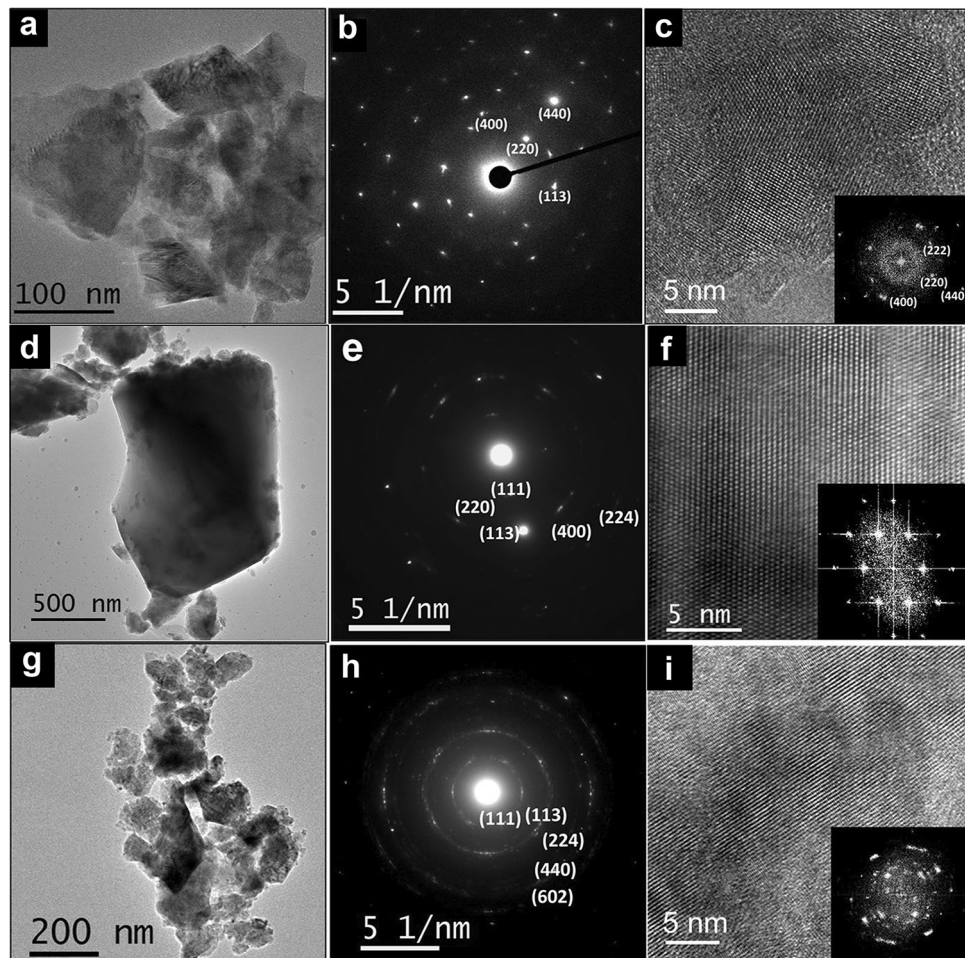


Fig. 8 **a** Bright field low magnification TEM image of the High-Cr magniochromite (Type I) and **b** its corresponding selected area electron diffraction (SAED) and **c** high-resolution TEM image [corresponding fast Fourier transform (FFT) (inset figure)] show the crystalline spots attributed to the (220), (113), (400) and (440) planes of chromite [JCPDS 01-089-2618]. **d** Bright field low magnification TEM image of the Medium-Cr ferrichromite (Type II) and **e** corresponding selected area electron diffraction (SAED) show (111), (220), (113), (400) and (224) planes of chromite [JCPDS 01-089-

2618] and **f** High-resolution TEM image [corresponding fast Fourier transform (FFT) (inset figure)] confirms the crystalline nature of the sample. **g** Bright field low magnification TEM image of the Low-Cr ferrichromite (Type III) and **h** corresponding selected area electron diffraction (SAED) show (111), (113), (224), (440) and (602) planes of chromite structure [JCPDS 01-089-2618], and **i** High-resolution TEM image [corresponding fast Fourier transform (FFT) (inset figure)] confirms the crystalline nature of ferrichromite

low FeO (12.5–17.7 wt.%) and low TiO₂ (0.15–0.19 wt.%). It hosts very low quantities of trace elements which demonstrates the original/primary magmatic characteristics. When the trivalent cations (Al-Cr-Fe³⁺) of Type I chromite are plotted into a ternary diagram (Barnes and Roeder 2001), all chromite compositions fall in an overlapping narrow field that conforms to a komatiitic and boninitic source (Fig. 10). Many studies have also indicated that there is a direct relation between the FeO/MgO ratios, the TiO₂ and Al₂O₃ contents of the chromite and its parental melt that can be assessed based on the liquidus spinel composition (e.g. Maurel and Maurel 1982; Kamenetsky et al. 2001). Cumulus chromites from massive chromitites might be slightly compositionally modified due to equilibration with olivine

(Irvine 1965, 1967; Dick 1977). Therefore, we have only used the composition of unaltered chromite grains to estimate the composition of the parent melt. Calculated from the chromite compositions, the FeO/MgO ratio of the parent liquid would have varied between 0.57 to 0.97. Based on the equation proposed by Maurel and Maurel (1982), the Al₂O₃ content of the melt is then calculated to be in the range of 9.11 to 11.26 wt.%. The Cr-number versus Mg-number plots also suggest a boninitic or komatiitic parentage for these chromites (Fig. 11). Boninites and komatiites are very similar in terms of their major oxide compositions and their trace element contents are somewhat similar (Barnes et al. 2020). There are several studies where the evolution of boninite from a komatiitic parental melt either by crustal

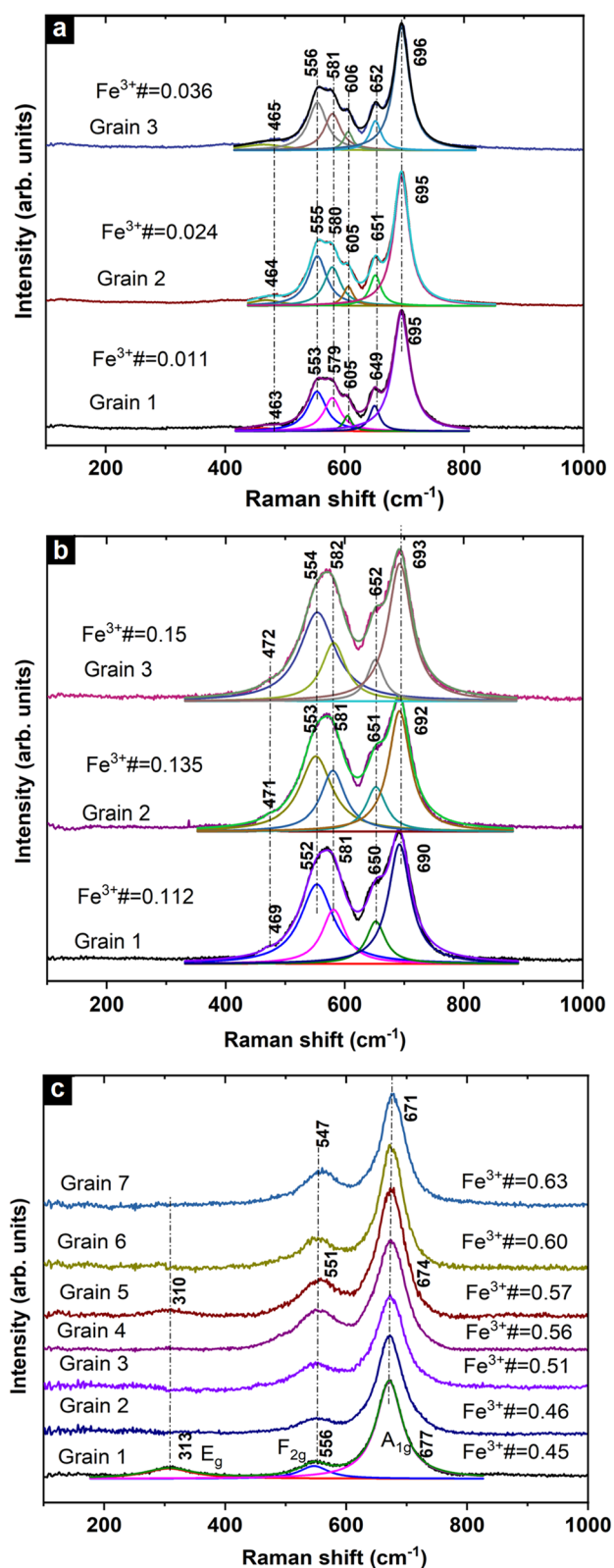


Fig. 9 Raman spectra of: **a** magnesiochromite (Type I), **b** intermediate type ferrian chromite (Type II) and **c** ferrichromite (Type III). The values of Raman bands are quoted for different grains that were randomly chosen

contamination or fractional crystallization have been suggested (e.g. Barley 1986; Sun et al. 1989). The Type I chromite compositions have slightly higher concentrations of trace elements (Sc, Mn, Co, V, Zn) compared to MORB melts and their trace-element patterns are similar to those of boninites (data compared with Pagé 2001, 2006 and Pagé and Barnes 2009). Hence the parent melt type for the Type I chromite could be boninitic. A boninitic parentage of the chromites of the adjacent Nuasahi massif has also been suggested by Pal and Mitra (2004) and Mondal et al. (2006). Based on plots of TiO_2 versus Al_2O_3 , Kamenetsky et al. (2001) have identified several fields, where the compositions of the spinels are distinguished based on their mode of occurrence and tectonic setting. These criteria would suggest that the Bangur chromitite bodies have formed in a back-arc and supra-subduction zone peridotite setting (Fig. 12). Compared to the Type I chromite, the Type II chromite (ferrian chromite) contains less Cr_2O_3 and MgO but has more FeO, Fe_2O_3 , Al_2O_3 and TiO_2 (Table 1). This type of change in chromite composition can be expected because the residual melt would have become richer in Fe, Al and Ti after crystallization of the Type I chromite which forms the major ore bodies in this area. The Type II chromites are also enriched in almost all measured trace elements (e.g. V, Mn, Co, Cu, Ga, Nb, Pb; Table 2). This indicates that melts crystallizing the Type II chromite are chemically more evolved and the ferrian chromite have formed later than the Type I chromite.

Hydrothermal alteration of primary chromites

Chromite belonging to the spinel family ($\text{A}^{2+}\text{B}^{3+}_2\text{O}_4$) exhibits a wide-range of compositions because of cationic substitutions such as Mg, Fe, Mn, Al, Ti etc. in both A and B sites. Substitution of Fe^{3+} can occur to a large extent that gives rise to iron-rich chromites which are referred to as ferrian chromite or “ferritchromite”. The term ‘*ferritchromit*’ (in German) was coined by Spangenberg (1943) to describe an altered variety of chromite enriched in ferric iron content from a chromite deposit at Zobten (i.e. Sobótka, now in Poland). Some authors have also used the term ferritchromite to describe a two-phase intergrowth of spinels (e.g. Wylie et al. 1987; Shen et al. 1988; Mitra et al. 1992; Burkhard 1993). Although the term ferritchromite has not been formally approved by IMA, it is still frequently used in the recent literature (e.g. Augé and Lerouge 2004; Merlini et al. 2009; Jena et al. 2016; Bhat et al. 2019; Hodel et al. 2020; Nayak et al. 2021). However, in this paper we have consistently used the terms ferrian chromite and ferrichromite strictly following the IMA nomenclature.

It is a very common observation that chromite alters to ferrian chromite during serpentinization, chloritization, hydrothermal alteration and/or metamorphism (Ulmer 1974;

Table 4 Raman bands of magnesiochromite (Type I), ferrian chromite (Type II) and ferrichromite (Type III) and their assignments

Mineral	Fe ³⁺ #	Assignment					
		$\nu_1(A_{1g})$			$\nu_3(F_{2g})$	$\nu_4(F_{2g})$	$\nu_2(E_g)$
Magnesiochromite	0.011	695	649	605	579	553	463
Ferrian chromite	0.112	690	650		581	552	469
Ferrichromite	0.45	677				556	313

Evans and Frost 1975; Bliss and MacLean 1976; Frost 1991; Burkhard 1993; Abzalov 1998; Barnes 2000; Proenza et al. 2004; González-Jiménez et al. 2009; Mukherjee et al. 2010; Gervilla et al. 2012). However, the oxygen fugacity-pH and P-T conditions of formation would vary. In our study area, two distinct varieties of Fe³⁺ bearing chromite occur: 1) A partially altered chromite that has formed at low temperature related to serpentinization/chloritization which shows a ring-pattern with diffused alteration and has a variable chemical composition from centre to periphery with relatively low and variable Fe³⁺; 2) A second variant that is the product of relatively high-temperature hydrothermal alteration where the chromite grains are completely altered with very high Fe³⁺ content. In this case the chemical composition remains more or less uniform within narrow limits in a single chromite grain.

Low-temperature hydrothermal alteration

The development of a ferrian chromite rim (that has a composition similar to that of Type II) can be interpreted either as 1) an alteration product of the original chromite, or 2)

an overgrowth formed on the outer surface of the original chromite. The formation mechanism of the former process could be either solid state inter-diffusion in which Mg, Al, Cr diffuse out from the parent chromite and Fe ions migrate inwards or a dissolution-precipitation reaction. Formation of the ferrian chromite rim as an overgrowth would occur by release of Fe and Mg ions from surrounding silicates and precipitation of the secondary overgrowth on original chromite grains. This would involve dissolution of chromite at the grain boundaries during serpentinization and reprecipitation of the dissolved Cr and Fe to form ferrian chromite first and then magnetite on the parent chromite. Mohanty et al. (1996)

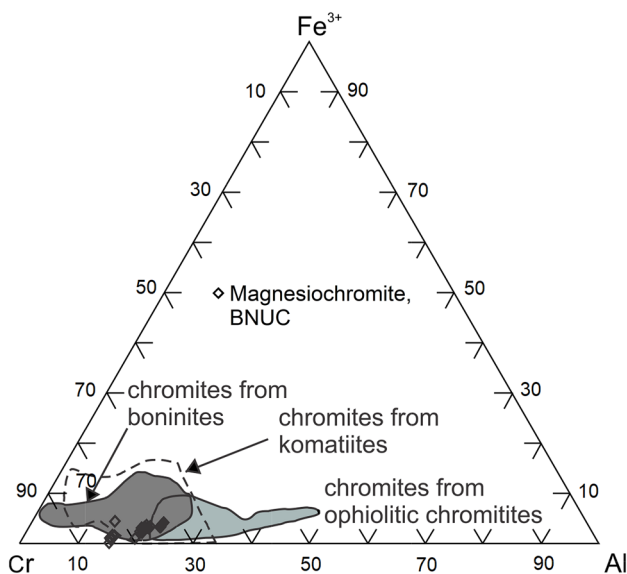


Fig. 10 Trivalent cation (%) plot of massive magnesiochromites (Type I) of BNUC (open diamonds) in comparison with chromites associated with boninites, ophiolites and komatiites (fields after Stevens 1944; Barnes and Roeder 2001)

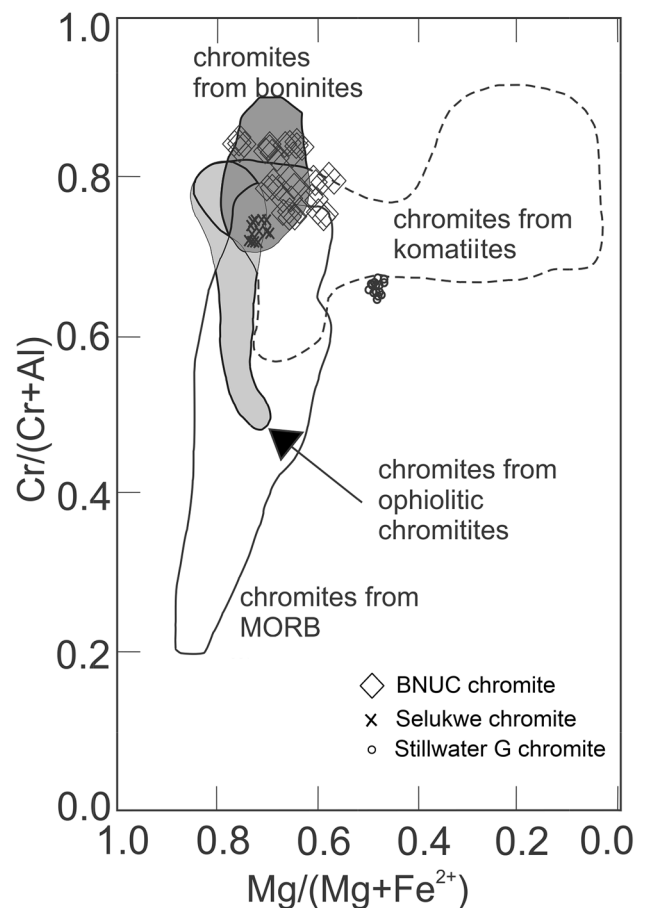


Fig. 11 Cr#-Mg# variations in primitive chromite compositions (open diamonds) from BNUC compared to some other Archean occurrences (black cross - Selukwe chromite; open circle - Stillwater G chromite). Fields after Rollinson (1995)

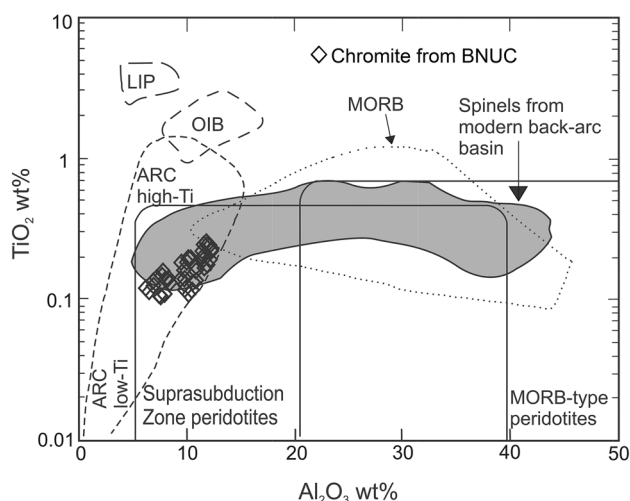
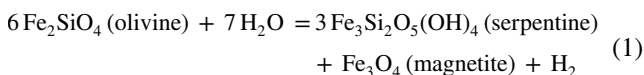


Fig. 12 TiO_2 vs Al_2O_3 variations seen in Cr-spinels of BNUC (open diamonds) with respect to modern day tectonic setting (after Kamenetsky et al. 2001)

have studied such chromite alterations of the Boula-Nuasahi area and proposed that the alteration is due to solid-state diffusion of elements from chromite outwards during serpentinization. If this interpretation would be correct, it would have problems in explaining some of the key observations related to the formation of the ferrian chromite rim. These are 1) the textural observation that the chromite grains become smooth at grain boundaries and become rounded; 2) the presence of gradational boundaries between ferrian chromite rims and the magnetite; 3) the presence of magnetite in the fractures of some chromite grains that have undergone similar alteration and have not developed ferrian chromite rims.

Our observations strongly suggest that both processes, solid-state diffusion and formation of new overgrowth, contributed to the formation of the ferrian chromite rims. The magnetite rim developed around chromite cannot be attributed to have formed only from precursor chromite. Irrespective of whether the Fe-Mg rock contains chromite or not, serpentinization commonly produces magnetite (Frost 1985; Sleep et al. 2004; Evans et al. 2013; McCollom and Seewald 2013; Nayak and Meyer 2015). This is attributed to a strongly reducing environment which is generated by the serpentinization reaction that produces significant hydrogen:



Based on the results of our study, the formation of ferrian chromite was not controlled by some preferred crystallographic orientation. Since the alteration is observed to occur mainly along grain boundaries and fractures through which grain-fluid interaction can easily occur, it can be attributed to a late post-magmatic hydrothermal stage.

The serpentinization process itself requires fluid activity, and during this hydrothermal stage the chromite grains are altered. Petrographic evidences suggest that the ferrian chromite formation was due to a combination of initial serpentinization that also caused the development of magnetite rims around chromite, followed by later metamorphism of the assemblage and reaction of the magnetite rims with the chromite to produce the Al- and Mg-poor ferrian chromite rim. Therefore, we propose that there was dissolution and subsequent reprecipitation of the dissolved Cr and Fe to form ferrian chromite first and subsequently growth of magnetite on the parent chromite along the grain boundaries during serpentinization. The chromites are modally insignificant, and are surrounded by hydrous magnesian silicates with which they can easily exchange cations through diffusion (Burkhard 1993). The released Cr and Al can be traced in the composition of associated chlorite that shows around 0.5 wt.% (max. 0.9 wt.%) Cr_2O_3 and 13.5 wt.% (max. 19.4 wt.%) Al_2O_3 . This type of alteration is very prominent in the accessory chromite grains in dunite and peridotite rocks but is not observed in the massive ores. The reason for not having such alterations in massive chromitite could be due to lack of required quantity of low-temperature hydrothermal fluid considering the large volume of massive ores that consist of closely packed chromite grains. The modal abundance of Fe-Mg silicates is extremely low and insignificant in the massive chromitite bodies. Therefore, the low-temperature hydrothermal alteration of chromite could not happen in the massive ores.

High-temperature hydrothermal alteration

The Type III chromite (ferrichromite) contains very low Cr_2O_3 , MgO and Al_2O_3 but the FeO, Fe_2O_3 , and TiO_2 contents are quite high (Table 1). These ferrichromites are exceptionally rich in all the measured trace elements (Table 2; Fig. 7). The EPMA and LA-ICP-MS data show that the concentrations of all minor and trace elements vary in a wide range, even in different chromite grains within the same sample. Both the petrographic characteristics (see "Petrography and textures of chromite" section and Fig. 5) and the chemical composition suggest that the ferrichromites have undergone post- and late-magmatic modifications where Cr, Mg and Al have been released from chromite and more Fe and Ti have been incorporated into their structure. Their major element composition and high trace element content can be correlated with the magmatic-hydrothermal event linked to the late-stage intrusion of the Bangur gabbro in this area. It is reasonably well established that the Bangur gabbro was intrusive into the ultramafic suite and injected into a shear zone forming a magmatic breccia that carried clasts from the previously formed ultramafics comprising dunite, pyroxenite and chromitite (Mondal et al. 2001; Augé

et al. 2002b; Augé and Lerouge 2004). This episode was followed by late magmatic-hydrothermal activity that altered the Fe-Mg silicates into hydrous phases such as amphibole and mica, and the composition of chromite in the chromite clasts was altered to iron-rich chromite.

The TiO_2 contents of these ferrichromites are exceptionally high and quite variable (0.5 to 17.17 wt.%) which points to significant hydrothermal mobility of Ti. This places some important constraints on the chemical character of the hydrothermal fluid that was responsible for the alteration of the magmatic chromite and the mobilization of Ti. The solubility of Ti in hydrothermal fluids is lowest at near-neutral pH, but significantly higher at acidic or alkaline pH. Furthermore, special ligands such as fluoride can strongly enhance the solubility of Ti in hydrothermal fluids (e.g. Ryzhenko et al. 2006). Reaction of hydrothermal fluids with mafic to ultramafic rocks causes the pH to become alkaline, and extensive serpentinization releases significant quantities of hydroxyl ions and can drive the pH up to value as high as 10 (e.g. Twing et al. 2017, and references therein). At such elevated pH conditions, the solubility of Ti would be enhanced by two to three orders of magnitude compared to neutral pH for the same temperatures and pressures.

Breakdown of primary Fe-Mg phases such as clinopyroxene and magmatic amphibole, which commonly host significant Ti in ultramafic rocks, would have liberated the Ti that would then become incorporated into the newly formed ferrichromites. We have analyzed the Ti content of the magmatic silicate phases clinopyroxene (TiO_2 : 0.05–1.39 wt.%) and magmatic amphibole (TiO_2 : 2.81–2.86 wt.%). They are significantly higher than the Ti contents of the secondary hydrous silicate phases chlorite and serpentine whose TiO_2 contents are extremely low (<0.01 wt.%). It has also been reported that the composition of the breccia apophysis (which is an alteration product of Bangur gabbro) is more mafic than the original Bangur gabbro (Augé and Lerouge 2004). This is due to the assimilation of more dunite and peridotite fragments during the brecciation. The secondary silicate phases such as biotite and amphibole that formed during this late-hydrothermal alteration stage contains less Ti than what would be expected for magmatic biotite in mafic-ultramafic complexes (Augé and Lerouge 2004). These data strongly support the model where high pH fluids formed by serpentinization reactions mobilized the Ti, leading to the formation of ferrichromite enriched in Ti and hydrous silicate phases depleted in Ti.

Structural changes in chromite

The normal spinel structure consists of a F-centered cubic close-packed array of oxygen atoms with trivalent cations occupying half of the octahedral interstices and divalent

cations occupying one eighth of the tetrahedral interstices (Wang et al. 2004). The inverse spinel structure implies that the A-sites are occupied by Fe^{3+} ions, while an equal number of Fe^{2+} and Fe^{3+} ions share the B-site. The B-site retains the local D_{3d} symmetry without lowering of symmetry due to the delocalized nature of electrons (Shebanova and Lazor 2003). In the Type II ferrian chromite, marginal increases in Raman shifts are observed for all bands because of the increasing content of the heavier Fe^{3+} ions relative to Cr (Fig. 9). The possible explanation for this behavior is an increase in the inversion parameter as the rise in Fe^{3+} content results in a decrease in the lattice parameter which could be attributed to the tetrahedrally coordinated Fe^{3+} having a smaller ionic radius than the Mg^{2+} ion (Shannon 1976; Kharbish 2018). The Raman bands of Type III ferrichromite match well with the Raman bands of magnetite mineral (Shebanova and Lazor 2003) indicating inverse nature of spinel structure in ferrichromite. This shows the usual red shift trend in Raman bands with increasing content of the heavier Fe^{3+} ions on different grains.

Conclusions

In the Boula-Nuasahi ultramafic complex of India, five morphological varieties of chromite ores are identified in the Bangur chromite deposit, which are massive, spotted, banded, disseminated, and breccia types. Chromite compositions of all the above ore varieties fall into three chemical types such as high-Cr chromite, medium-Cr chromite (ferrian chromite) and low-Cr & high-Fe chromite (ferrichromite). The chemical compositions of pristine magnesiochromite (high-Cr) and their Cr-number versus Mg-number plots indicate that this chromite deposit has originated dominantly from a boninitic magma. Post-magmatic hydrothermal processes have altered the chemical compositions of magmatic chromite. While the low-temperature (~100–200 °C) hydrothermal alteration in the ultramafic rocks partially altered the chromite developing a core-rim type structure with an intermediate ferrian-chromite rim and an outer magnetite rim, interaction with high-temperature (500–600 °C) hydrothermal fluids was responsible for the complete conversion of original primary chromites of different ore-types into ferrichromite. Despite large variations in chemical composition, all the three types of chromite have FCC crystallographic structure. However, there is a systematic change of structure from normal spinel-type (high-Cr magnesiochromite) to inverse spinel-type (ferrichromite) through an intermediate medium-Cr chromite. Completely altered chromite grains with high Fe^{3+} content (ferrichromite) and having almost uniform chemical composition are formed due to high-temperature hydrothermal

alteration and serpentinization reactions creating high pH fluids. These have efficiently mobilized and transported Ti as shown by the drastic depletion of Ti content in the altered hydrous phases (serpentine, chlorite).

Supplementary Information The online version contains supplementary material available at <https://doi.org/10.1007/s00710-024-00856-3>.

Acknowledgements B. Nayak is indebted to the Alexander von Humboldt Foundation, Germany for a Humboldt fellowship in the revisit scheme to work at the Institute of Applied Mineralogy and Economic Geology, RWTH Aachen University, Germany. R. Debata received a research fellowship from DST, Govt. of India under the INSPIRE scheme. The authors are thankful to M/s Odisha Mining Corporation Ltd., Bhubaneswar for extending permission to work in its Bangur mining leasehold area and collect ore and rock samples.

References

- Abzalov MZ (1998) Chrome–spinel in gabbro–wehrlite intrusions of the Pechenga area, Kola Peninsula, Russia: emphasis on alteration features. *Lithos* 43:109–134
- Augé T, Bailly L, Cocherie A, Genna A, Guerrot C, Lerouge C, Mukherjee MM, Patra RN (2002a) Magmatic and hydrothermal platinum-group element mineralization in the Baula area, Orissa, India. In: Boudreau. A. (Ed.), Proceedings of the 9th International Platinum Symposium, July 2002, Billings, USA 21–24
- Augé T, Salpeteur I, Bailly L, Mukherjee MM, Patra RN (2002b) Magmatic and hydrothermal platinum-group minerals and base-metal sulfides in the Baula Complex, India. *Can Mineral* 40(2):277–309
- Augé T, Lerouge C (2004) Mineral-chemistry and stable-isotope constraints on the magmatism, hydrothermal alteration, and related PGE - (base-metal sulphide) mineralisation of the Mesoarchean Baula-Nuasahi Complex, India. *Min Deposita* 39:583–607
- Barley ME (1986) Incompatible-element enrichment in Archean basalts: a consequence of contamination by older sialic crust rather than mantle heterogeneity. *Geology* 14:947–950
- Barnes SJ (1998) Chromite in komatiites, I. Magmatic controls on crystallization and composition. *J Petrol* 39:1689–1720
- Barnes SJ (2000) Chromite in komatiites, II. Modification during greenschist to mid-amphibolite facies metamorphism. *J Petrol* 41:387–409
- Barnes SJ, Mansur E, Pagé P, Meric J, Arguin JP (2020) A comparison of major and trace element compositions of chromites from the Stillwater, Bushveld and Great Dyke layered intrusions with chromites from komatiites, boninites and large igneous provinces. EGU General Assembly 2020, Online, 4–8 May 2020, EGU2020-9768. <https://doi.org/10.5194/egusphere-egu2020-9768>
- Barnes SJ, Roeder PL (2001) The range of spinel compositions in terrestrial mafic and ultramafic rocks. *J Petrol* 42:2279–2302
- Bhat IM, Ahmad T, Rao DVS (2019) Alteration of primary Cr-spinel mineral composition from the Suru Valley ophiolitic peridotites, Ladakh Himalaya: their low-temperature metamorphic implications. *J Earth Syst Sci* 128:1–14
- Bliss NW, MacLean WH (1976) The paragenesis of zoned chromite from central Manitoba. In: Chromium: its Physicochemical Behavior and Petrologic Significance, Papers from a Carnegie Institution of Washington Conference, Geophysical Laboratory, pp 973–990
- Bosi F, Biagioni C, Pasero M (2019) Nomenclature and classification of the spinel group. *Eur J Mineral* 31:183–192
- Burkhard DJM (1993) Accessory chromium spinels: their coexistence and alteration in serpentinites. *Geochim Cosmochim Acta* 57:1297–1306
- Chakraborty KL (1958) Chromite ores associated with ultrabasic rocks of Nausahi, Keonjhar Dist., Orissa, India—their mineralogy and genesis. *Proc Nat Inst Sci India* 24A:78–88
- Chatterjee SC (1945) The gabbro rocks found near Gorumahisani Pahar. *Proc Natl Inst Sci India* 11:255–282
- Dick HJB (1977) Partial melting in the Josephine Peridotite; I, the effect on mineral composition and its consequence for geobarometry and geothermometry. *Am J Sci* 277(1):801–832
- Evans BW, Frost BR (1975) Chrome-spinel in progressive metamorphism—a preliminary analysis. *Geochim Cosmochim Acta* 39:959–972
- Evans BW, Hattori K, Baronnet A (2013) Serpentinite: what, why, where? *Elem* 9:99–106
- Frost BR (1985) On the stability of sulfides, oxides, and native metals in serpentinite. *J Petrol* 26:31–63
- Frost BR (1991) Introduction to oxygen fugacity and its petrologic importance. *Rev Miner* 25(1):1–9
- Gervilla F, Padrón-Navarta JA, Kerestedjian T, Sergeeva I, Gonzalez-Jimenez JM, Fanlo I (2012) Formation of ferrian chromite in podiform chromitites from the Golyamo Kamenyane serpentinite, Eastern Rhodopes, SE Bulgaria: a two-stage process. *Contrib Mineral Petrol* 164:643–657
- González-Jiménez J, Gervilla F, Proenza JA, Kerestedjian T, Augé T, Bailly L (2009) Zoning of laurite (RuS₂) - erlichmanite (OsS₂): implications for the origin of PGM in ophiolite chromitites. *Eur J Mineral* 21(1):419–432
- Grimes NW, Collett AJ (1971) Correlation of infra-red spectra with structural distortions in the spinel series mg(Cr_xAl_{2-x})O₄. *Phys Status Solidi* 43:591–599
- Guillong M, Meier DL, Allan MM, Heinrich CA, Yardley BWD (2008) SILLS: a Matlab-based program for the reduction of laser ablation ICP-MS data of homogeneous materials and inclusions. *Miner Assoc Can Short Course* 40:328–333
- Hodel F, Macouin M, Trindade RIF, Araujo JFDF, Respaud M, Meunier JF, Cassayre L, Rousse S, Drigo L, Schorne-Pinto J (2020) Magnetic properties of ferritchromite and Cr-magnetite and monitoring of Cr-spinels alteration in ultramafic and mafic rocks. *Geochem Geophys Geosyst* 21(11):1–21
- Irvine TN (1965) Chromian spinel as a petrogenetic indicator: part 1. Theory. *Can J Earth Sci* 2:648–672
- Irvine TN (1967) Chromian spinel as a petrogenetic indicator: part 2. Petrologic applications. *Can J Earth Sci* 4:71–103
- Jena MS, Mohanty JK, Venugopal R, Mandre NR (2016) Characterization of low grade PGE ores of Boula-Nuasahi Area, Odisha, India and implication on beneficiation. *Ore Geol Rev* 72:629–640
- Kamenetsky VS, Crawford AJ, Meffre S (2001) Factors controlling chemistry of magmatic spinel: an empirical study of associated olivine, Cr-spinel and melt inclusions from primitive rocks. *J Petrol* 42:655–671
- Kharbish S (2013) Metamorphism and Geochemical aspects on neo-proterozoic serpentinites hosted chrome spinel from Gabal Al-Degheimi, Eastern Desert, Egypt. *Carpathian J Earth Environ Sci* 8:125–138
- Kharbish S (2018) Raman spectroscopic features of Al-Fe³⁺-poor magnesiochromite and Fe²⁺-Fe³⁺-rich ferrian chromite solid solutions. *Mineral Petrol* 112:245–256
- Khatun S, Mondal SK, Zhou MF, Balaran V, Prichard HM (2014) Platinum-group element (PGE) geochemistry of Mesoarchean ultramafic-mafic cumulate rocks and chromitites from the Nuasahi Massif, Singhbhum Craton (India). *Lithos* 205:322–340
- Maurel C, Maurel P (1982) Etude Experimentale De La Solubilite Du chrome dans les bains silicates basiques et de sa distribution entre Liquide et mineraux coexistants: conditions d'existence Du Spinelle Chromifere. *Bull Mineral* 105:640–647
- McCullom TM, Seewald JS (2013) Serpentinites, hydrogen, and life. *Elements* 9:129–134

- Merlini A, Grieco G, Diella V (2009) Ferritchromite and chromian-chlorite formation in mélange-hosted Kalkan chromitite (southern urals, Russia). *Am Mineral* 94:1459–1467
- Mindat.org: <https://www.mindat.org/min-1036/min-10656/min-43494>
- Mitra S, Pal T, Maity PK, Moon H-S (1992) Ferritchromite and its optochemical behaviour. *Mineral J* 16:173–186
- Mohanty JK, Paul AK, Sahoo RK (2001) Sequence of chromite crystallization at Boula-Nausahi igneous complex, Orissa, India. *Mineralogica-Petrographica* 42:37–45
- Mohanty JK, Sahoo RK (1989) Chemistry of chromites from Boula-Nausahi Igneous Complex, Keonjhar district, Orissa and its petrogenetic significance. *J Geol Soc India* 33:321–331
- Mohanty JK, Sahoo RK, Paul AK (1996) Chromite alteration at Boula-Nausahi igneous complex, Orissa. *J Geol Soc India* 48:265–276
- Mondal SK, Baidya TK, Gururaja Rao KN, Glascock MD (2001) PGE and Ag mineralization in a breccia zone of the precambrian nausahi ultramafic-mafic complex, Orissa, India. *Can Mineral* 39:979–996
- Mondal SK, Ripley EM, Li C, Frei R (2006) The genesis of archaean chromitites from the Nausahi and Sukinda massifs in the Singhbhum Craton, India. *Precambrian Res* 148:45–66
- Mukherjee S (1969) Clot textures developed in the chromitites of Nausahi, Keonjhar District, Orissa, India. *Econ Geol* 64:329–337
- Mukherjee S (1962) Geology, mineralogy and geochemistry of the chromite deposits of Nausahi, Keonjhar dist. Odisha, *QJ Geol Min Met Soc India* 34(1):29–45
- Mukherjee R, Mondal SK, Rosing MT, Frei R (2010) Compositional variations in the Mesoarchean chromites of the Nuggihalli schist belt, Western Dharwar Craton (India): potential parental melts and implications for tectonic setting. *Contrib Mineral Petrol* 160:865–885
- Mukhopadhyay D (2001) The archaean nucleus of Singhbhum: the present state of knowledge. *Gondwana Res* 4:307–318
- Nayak B, Meyer FM (2015) Tetrataenite in terrestrial rock. *Am Mineral* 100:209–214
- Nayak B, Sindern S, Wagner T (2021) Formation of late-stage hydrothermal mineralization in the Mesoarchean Boula-Nausahi ultramafic complex, Odisha, India: constraints from arsenopyrite geothermometry and trace element data. *Ore Geol Rev* 139:104482
- Pagé P (2001) L'origine de la distribution des teneurs en EGP dans les faciès mantelliques océaniques et ophiolitiques: exemples de la faille transformante Garrett, Pacifique sud et du massif de North Arm Mountain, complexe ophiolitique de Bay of Islands, Terre-Neuve, Canada, M.Sc. thesis, Laval University, Québec, p 414. <http://hdl.handle.net/20.500.11794/35028>
- Pagé P (2006) Pétrogenèse de l'ophiolite de Thetford Mines, Québec, Canada, avec un accent particulier sur les roches du manteau et les chromitites. Thesis, Quebec, University of Quebec, National Institute of Scientific Research, Doctorate in Earth Sciences, p 299
- Pagé P, Barnes SJ (2009) Using Trace Elements in chromites to constrain the origin of Podiform chromitites in the Thetford Mines Ophiolite, Québec, Canada. *Econ Geol* 104:997–1018
- Pal T, Mitra S (2004) P–T–fO₂ controls on a partly inverse chromite-bearing ultramafic intrusive: an evaluation from the Sukinda Massif, India. *J Asian Earth Sci* 22:483–493
- Pronza JA, Ortega-Gutiérrez F, Camprubi A, Tritlla J, Elías-Herrera M, Reyes-Salas M (2004) Paleozoic serpentinite-enclosed chromitites from Tehuizingo (Acatlán Complex, southern Mexico): a petrological and mineralogical study. *J South Am Earth Sci* 16:649–666
- Rollinson H (1995) The relationship between chromite chemistry and the tectonic setting of Archaean ultramafic rocks. In: Blenkinsop TG, Tromps P (eds) *Sub-Saharan*. Balkema, Econ. Geol. Amsterdam, pp 7–23
- Ryzhenko BN, Kovalenko NI, Prisyagina NI (2006) Titanium complexation in hydrothermal systems. *Geochem Internat* 44:879–895
- Saha AK (1994) Crustal evolution of Singhbhum-North Orissa, Eastern India. *Mem Geol Surv India* 27:341
- Shannon RD (1976) Revised effective ionic radii and systematic studies of interatomic distances in halides and chalcogenides. *Acta Cryst A* 32:751–767
- Shebanova ON, Lazor P (2003) Raman spectroscopic study of magnetite (FeFe₂O₄): a new assignment for the vibrational spectrum. *J Solid State Chem* 174:424–430
- Shen P, Hwang S-L, Chu H-T, Jeng R-C (1988) STEM study of ferritchromite from the Heng-Chun Chromitite. *Am Mineral* 73:383–388
- Sleep NH, Meibom A, Fridriksson T, Bird DK (2004) H₂-rich fluids from serpentinization: geochemical and biotic implications. *Proc Natl Acad Sci* 101:12818–12823
- Spangenberg K (1943) Die Chromitlagerstätte Von Tampadel Am Zobten. *Z Prakt Geol* 51:13–35
- Stanton RL (1972) *Ore Petrology*. McGraw-Hill, New York, 713 p
- Stevens RE (1944) Composition of some chromites of the western hemisphere. *Am Mineral* 29:1–34
- Sun SS, Nesbitt RW, McCulloch MT (1989) Geochemistry and petrogenesis of Archaean and early Proterozoic siliceous high-magnesian basalts. In: Crawford AJ (Ed.) *Boninites and Related Rocks*. Unwin Hyman (publ.), pp 148–173
- Thayer TP (1960) Some critical differences between alpine-type and stratiform peridotite-gabbro complexes. 21st intern. Geol. Congress, Copenhagen, XIII, pp 247–259
- Twing KI, Brazelton WJ, Kubo MDY, Hyer AJ, Cardace D, Hoehler TM, McCollom TM, Schrenk MO (2017) Serpentinization-influenced groundwater harbors extremely low diversity microbial communities adapted to high pH. *Front Microbiol* 8:308
- Ulmer GC (1974) Alteration of chromite during serpentinization in the Pennsylvania-Maryland district. *Am Mineral* 59:1236–1241
- Wang A, Kuebler KE, Jolliff BL, Haskin LA (2004) Raman spectroscopy of Fe-Ti-Cr-oxides, case study: martian meteorite EETA79001. *Am Mineral* 89:665–680
- Whitney DL, Evans BW (2010) Abbreviations for names of rock-forming minerals. *Am Mineral* 95:185–187
- Wylie AG, Candela PA, Burke TM (1987) Compositional zoning in unusual Zn-rich chromite from the Sykesville District of Maryland and its bearing on the origin of ferritchromite. *Am Mineral* 72:413–422

Publisher's Note Springer Nature remains neutral with regard to jurisdictional claims in published maps and institutional affiliations.

Springer Nature or its licensor (e.g. a society or other partner) holds exclusive rights to this article under a publishing agreement with the author(s) or other rightsholder(s); author self-archiving of the accepted manuscript version of this article is solely governed by the terms of such publishing agreement and applicable law.